Theses and Dissertations

1972

The effects of heat treatment on the electro-optical properties of (Zn, 0) doped GaP diodes

Robert A. Worden
Lehigh University

Follow this and additional works at: https://preserve.lehigh.edu/etd

Part of the Materials Science and Engineering Commons

Recommended Citation

THE EFFECTS OF HEAT TREATMENT ON
THE ELECTRO-OPTICAL PROPERTIES
OF (Zn,O) DOPED GaP DIODES

by

Robert A. Worden

A Thesis

Presented to the Graduate Faculty

of Lehigh University

in Candidacy for the Degree of

Master of Science

in Metallurgy and Materials Science

Lehigh University

1972

CERTIFICATE OF APPROVAL

This thesis is accepted and approved in partial fulfillment
of the requirements for the degree of Master of Science.

May 11, 1972
Date

Michael R. Notis
Professor in Charge

C. P. Carard II
Chairman of the Department
of Metallurgy and Materials
Science

ACKNOWLEDGEMENTS

TABLE OF CONTENTS

TABLE OF CONTENTS (cont)

LIST OF TABLES

LIST OF FIGURES

LIST OF FIGURES (cont)

LIST OF FIGURES (cont)

ABSTRACT

Zn,O doped GaP light-emitting diodes were heat treated in the temperature range of 400 to 500°C. The effects of the low temperature annealing on the electrical and optical properties of the diodes were monitored by measuring the electroluminescent efficiency, emission spectra, junction capacitance-voltage and the forward current-voltage characteristics of the devices. The electroluminescent efficiency data and emission spectra revealed that annealing at low temperatures increases the total quantum efficiency and that the red emission increases relative to the infrared emission. Junction C-V measurements on unannealed diodes showed that the p and n regions were separated by a compensated layer ≈ 800 Å wide resulting in a p-π-n diode structure. Annealing increases the width of the π-layer and is attributed to the compensation of Te atoms in the n-layer by Zn atoms diffusing from the p-layer across the junction. Recombination of hole-electron pairs in the space charge region dominates the forward I-V characteristics of GaP diodes up to ≈ 1.6 volts. For larger bias a parallel mode recombination mechanism dominates the characteristic due to recombination occurring in the p-layer adjacent to the space charge region. Annealing reduces the current at a given voltage, resulting in an increase in the Shockley-Read lifetime $[\tau_{po}\tau_{no}]^{1/2}$.

-1-

I. INTRODUCTION

A. General

Since the observation of visible light emission from GaP[1,2], considerable interest has been generated in the use of this material for low-voltage, low-power indicator lamps and alphanumeric displays. GaP is a III-V compound semiconductor possessing the zinc-blende structure. The crystal property that has the greatest influence on electroluminescence is the energy separation between the valence and conduction bands; for visible emission to occur an energy gap, E_g, of 1.7 to 3.1 ev. is required. The minimum separation of the bands thus determines the maximum wavelength or color of the emitted light. The lattice constant, a_o, for GaP is approximately 5.451 Å and the energy gap, E_g, is 2.26 ev. both measured at $25^{\circ}C$[3]. Thus GaP is one of the few III-V compounds suitable for luminescence in the visible region.

Electroluminescence in a p-n junction diode occurs by radiative recombination of injected minority carriers with majority carriers while under a forward bias. Recombination can occur either radiatively with the emission of a photon of light or nonradiatively where energy is given up as a phonon. Since GaP has an indirect band gap, the minimum of the conduction band does not occur at the same momentum wave vector 'k' value as the maximum in the valence band; thus, band-to-band electron transitions require the emission or absorption of a phonon to conserve momentum along with the

emission or absorption of a photon. As a measure of the efficiency of the light-emission process, two quantities are defined. The internal quantum efficiency is the ratio of the number of minority carriers that recombine radiatively to the total number that recombine. However, a more meaningful quantity, especially for device applications, is the external quantum efficiency. This quantity is the ratio of the number of external emitted photons to the number of electrons flowing in the external circuit [3]. The internal and external quantum efficiencies differ by an amount due to absorption of photons in the bulk regions of the device or by reflections at the diode surfaces.

Previous studies have described the mechanisms of luminescence in Zn,O doped GaP [4-11]. Red luminescence occurs by two mechanisms:

    (1) recombination of electrons trapped at Zn-O centers with holes trapped at distant zinc sites (Pair Recombination) and

    (2) recombination of hole-electron pairs through excitonic emission.

The infrared emission is also accounted for by two processes:

    (1) recombination of electrons trapped at the donor oxygen sites with holes trapped at distant zinc acceptor sites (D-A Recombination) and

(2)   trapped electrons at oxygen sites with free holes

in the valence band (Bound-Free Recombination).

At room temperature excitonic and bound-to-free recombination

dominate the luminescent characteristics of GaP. Figure 1 is a

schematic of the electroluminescent process in GaP.

B.   P-N Junction Theory

To understand electroluminescence in light-emitting diodes

an elementary understanding of p-n junction behavior is required.

The n-region of the semiconductor contains mobile negative charges

(electrons) as the majority carrier and immobile positive donor

ions; while the p-region contains mobile positive charges (holes)

and immobile negative ions (acceptors). Only the mobile charges

(holes and electrons) enter into the conduction process since

they can accept energy upon application of an applied field. When

the n and p regions are brought into contact to form a junction,

holes and electrons diffuse due to the large concentration

gradients that exist. The diffusion of these mobile carriers

leaves a net positive charge of immobile donor ions in the n-region

near the interface and a net negative immobile charge due to

acceptor ions in the p-region near the interface. These im-

mobile charges set up an electric field that opposes further

diffusion of the mobile carriers. In thermal equilibrium, the

field balances the concentration gradient resulting in no net

current flow. The region near the junction containing the immobile

ions is nearly depleted of all mobile carriers and is called the junction space charge region.

In GaP red light-emitting diodes the p-region is either Zn or Cd doped with smaller quantities of the donor oxygen included. The Cd or Zn impurities provide a shallow acceptor level 0.064 ev above the top of the valence band while the oxygen provides a deep donor level approximately 0.895 ev below the bottom of the conduction band [8]. Figure 2a is an energy band diagram of a diode in equilibrium.

Application of a forward bias reduces the potential barrier and permits the flow of electrons and holes across the junction as exhibited in Figure 2b. The holes injected into the n-region as minority carriers, recombine with the majority carrier electrons, while on the p-side injected electrons recombine with holes. The dependence of the current flow with applied voltage is given by the expression:

$$I = I_o \exp (qV/nkT)$$

where k is the Boltzmann constant, T is the absolute temperature and n is a constant dependent upon the recombination mechanism. The value of I_o is constant for a given temperature and is independent of the applied voltage. For Zn,O doped GaP the red luminescence occurs within approximately a micron of the junction

in the p-region; therefore, electron injection from the n into the p layer controls the luminescence process. The injected electrons are trapped by a neutral complex resulting from an acceptor Zn and the donor O occupying nearest neighbor lattice sites [3]. The capture of the electron charges the Zn-O complex negatively and a hole is then captured by coulombic attraction. The electron and hole bound to the neutral complex are termed a bound exciton. The recombination of a hole-electron pair in this manner results in the emission of a photon of light in the red region of the visible spectrum.

C. Diffusion of Zinc in GaP

Chang and Pearson [12-14] observed that zinc behaves anomalously in GaP and other III-V compounds. The zinc diffusion profiles for temperatures greater than $900^\circ C$ were characterized by a very steep concentration gradient indicating a concentration dependence of the diffusion coefficient. They used Zn^{65} as a tracer and determined the diffusion coefficient from a Matano analysis and isoconcentration data. For temperatures below $900^\circ C$, the curves did not exhibit a steep gradient as was displayed for the higher temperatures, although the diffusion coefficient was found to be weakly concentration dependent. The expression for the concentration dependent diffusion coefficient is:

$$D = 7.5 \times 10^{-8} \, C_{Zn}^{0.45} \, \exp\left[\frac{-2.50}{kT}\right]$$

For temperatures greater than $900^\circ C$, it was found that D varied approximately as C_{Zn}^2 in the region between 5×10^{18} and 2×10^{19} cm^{-3}. To explain the behavior of Zn diffusion in GaP, Chang and Pearson invoked an interstitial-substitutional diffusion model that was previously suggested by Longini [15] for Zn in GaAs. They made the following assumptions in deriving the relationship between D and C:

1. substitutional zinc in the Ga sublattice is neutral or is a singly ionized acceptor

2. a small fraction of zinc exists interstitially and acts as a doubly ionized donor, the concentration being enhanced by the substitutional zinc acceptors

3. gallium vacancies remain neutral

4. diffusion occurs by both interstitial and substitutional modes with the interstitial mode being dominant at high zinc concentrations and temperatures.

D. Purpose

Numerous investigations have shown that the external quantum efficiency can be increased by a factor of 2 to 10 by annealing at temperatures in the $400-725^\circ C$ range [16-20] and that the red efficiency can be increased at the expense of the infrared quantum efficiency [17]. These studies have been conducted on

-7-

both bulk material and p-n junction diodes. However, the external quantum efficiency of a diode is not only a function of the number of Zn-O complexes but also the injection efficiency, orientation and other factors associated with the diode.

Since zinc acts as a shallow acceptor in GaP and is known to be a very fast diffuser, degradation of the junction properties of the diode would be expected due to out diffusion of zinc from the p-region to the n-region. Since the injection efficiency of a diode is proportional to the gradient of the carrier concentration, additional heat treatment after epitaxial growth should result in a reduced injection efficiency and thus, a decrease in the quantum efficiency. Low temperature annealing therefore produces two competing effects:

1. increases the concentration of Zn-O complexes in the p-region which tends to increase the quantum efficiency, and

2. decreases the Zn concentration gradient at the p-n junction which lowers the injection efficiency and therefore reduces the quantum efficiency.

The purpose of this study is therefore to investigate the effects of low temperature heat treatments on the electrical and optical properties of Zn,O doped GaP junction diodes and to explain these effects in terms of Zn diffusion in the regions near and across the p-n junction.

II. EXPERIMENTAL DETAILS

A. Crystal Growth and Diode Preparation

The material used in this investigation was grown on GaP substrates using a liquid-phase epitaxy technique at Bell Telephone Laboratories in Reading, Pennsylvania. The substrate material was approximately .012" thick and was selenium doped, an n-type impurity, to a concentration of 2-5 x 10^{17} cm^{-3}. Growth was in the <111> direction. After appropriate polishing and cleaning an n-type epitaxial layer, doped with tellurium, was grown on the substrate from the liquid phase. In this method Ga, GaP and Te are placed in one end of a quartz boat, which is contained in a quartz diffusion tube through which flows a reducing ambient gas. After heating the boat to the desired temperature, the boat is tipped so that the solution of GaP and Te in Ga covers the substrate at the opposite end of the boat. As the saturated solution cools, a thin Te doped GaP epitaxial layer is grown upon the substrate. Typical tipping temperatures and cooling rates are 1045°C and 3/4°C/min., respectively.

A p-layer doped with zinc and oxygen was then deposited on the n-layer, again employing the liquid-phase epitaxial process. Since the investigation is concerned with the effects of zinc diffusion on the junction and optical properties of diodes, zinc concentrations of 5 x 10^{17} and 1 x 10^{18} were desired. The

-9-

procedure for tipping the p-layer is similar to that previously described with the exception that the acceptor Zn replaces the donor Te and Ga_2O_3 additions are made to provide a source for oxygen incorporation. Thus the p-layer is intentionally doped with both types of impurities; however, the acceptor concentration is greater than the donor oxygen. To obtain the desired zinc concentrations, zinc additions of 0.04 mole percent and 0.07 mole percent were added to the melt. The Ga_2O_3 additions were held constant at 0.07 mole percent for both deposition runs. The boat was inserted into a diffusion furnace set at $500^{\circ}C$ containing a H_2 ambient and the temperature was increased until the desired tipping temperature was reached. Tipping occurred at approximately $1010^{\circ}C$ and the cooling rate was about $1^{\circ}C/min.$ during growth. The growth time was 18 minutes and the total time was approximately 105 minutes. To terminate growth the boat was flipped so the GaP substrates were not in contact with the Ga enriched solution. The furnace was then allowed to cool to about $500^{\circ}C$ and the boat was then removed. Figure 3 is a schematic representation of the tipping procedure.

Diodes were fabricated from the GaP wafers by contacting both the p and n-layers and then dicing the wafer into individual chips. Before evaporation of the contacts the wafers received the following treatment:

1. clean in hot conc. HNO_3 for 10 minutes

2. lightly polish p-layer using 1 micron Al_2O_3

3. lap n-type substrate to reduce total thickness to .012"

4. polish substrate using 1 micron Al_2O_3

5. degrease in boiling chloroform for 2 minutes

6. etch in chlorine saturated methanol solution for 45 seconds.

In the normal contacting procedure, the evaporated contacts are alloyed at $600^\circ C$ for 5 minutes in a nitrogen atmosphere. Since the annealing cycles for the diodes were to be carried out at temperatures less than $600^\circ C$, an alternate contact alloying procedure seemed advisable to eliminate the effects of the higher temperature. An attempt to alloy the contacts by elevating the temperature of the substrates during evaporation resulted in non-ohmic contacts with a forward voltage of 17 volts at 1 ma; therefore, it was decided to evaporate and alloy the contacts using a standard procedure so reliable contacts could be obtained.

The following evaporation procedure was followed:

1. evaporate 10,000 Å of a 2% Si-Au alloy on the n-substrate

2. evaporate 5,000 Å of a 1% Be-Au alloy on p-layer

3. evaporate 10,000 Å Au cap on p-layer

4. alloy contacts for 5 min. at $600^\circ C$ in dry nitrogen.

All evaporations were performed at a substrate temperature of

150°C. The contact geometries were obtained by evaporation through molybdenum masks. The Be-Au contacts were .005" diameter on .020" centers, while the Si-Au contacts were an array of .0015" dots on .0035" centers. The evaporations were conducted in the 3-4 x 10^{-7} Torr range.

After alloying the contacts were checked for linearity on a transistor curve tracer by probing between adjacent contacts. The wafers were then mounted on bakelite discs, p-side up, and partially cut approximately .004" deep forming .015" x .015" chips. The wafers were then etched in a 3:1:1 H_2SO_4:30% H_2O_2: H_2O solution maintained at 60°C for 5 minutes to remove damage resulting from the dicing operation.

B. Concentration Profile Measurements

Before fabrication of the wafers into diodes, doping concentration profiles in the wafers were obtained from capacitance-voltage measurements employing Schottky Barrier diodes evaporated on angle lapped surfaces. Previous investigations have described the procedure in determining doping concentrations employing Schottky analysis [21-24]. A small piece of each wafer was lapped on a 3° angle block using Linde #305 Al_2O_3 and was then polished with Linde A 0.3 micron polish. The specimens were etched in hot aqua regia (3:1 HCl:HNO_3) for 10 seconds prior to contacting. Contacts were formed by alloying 2% Zn doped and 2% Sn doped gold wires to the p and n-regions respectively using a carbon

resistance strip heater. The samples were stored in methanol
after the aqua regia etch and loaded wet into the chamber just
prior to contacting. The chamber was purged using 3% forming gas
prior to loading and during the alloying process. Two contacts
were formed on each region so that they could be checked for
linearity on a curve tracer. The contacts were protected with
apiezon wax and the samples again etched in warm 3:1 aqua regia
for 10 seconds. Just prior to loading the specimens in the
evaporator, they received a 60 second etch in room temperature
nitric acid and were then stored in methanol. The evaporator was
evacuated to 2×10^{-7} Torr before evaporation of the gold commenced.
A .004" dot pattern on .008" centers was generated by evaporation
through a molybdenum mask. Figure 4 is a sketch of the GaP sample
and the Au Schottky Barrier diodes.

Capacitance-Voltage measurements were conducted on the speci-
men using an automated test set designed at Western Electric,
Princeton, New Jersey. C-V measurements on a given diode consisted
of measuring the diode capacitance at a given voltage as the bias
was swept from $\approx$ + 0.400 volts to - 3.600 volts in 0.400
volt increments. Concentration profile measurements consisted
of making a series of C-V measurements on the evaporated diodes
along the lapped surface, starting at the surface of the p-layer.
As the p-n junction is traversed, the polarity of the probes must
be reversed and contact made to the n-type substrate. The raw

-13-

data was recorded on a 7-track magnetic tape using a Kennedy Model 1600 tape recorder for later processing on a Digital Equipment PDP-10 computer. The doping concentrations were determined from the expression:

$$\frac{d(\frac{1}{C})^2}{dV} = \frac{-2}{q\epsilon} \cdot \frac{1}{N^*}$$

where

ϵ = dielectric permittivity

q = electronic charge

C = diode capacitance per unit area

V = applied voltage

N^* = net doping concentration.

The concentration determined from C-V measurements, N^*, is the net impurity concentration; i.e., the difference between the donor and acceptor concentrations $\left| N_D - N_A \right|$. By knowing the spacing between diodes and the angle θ (shown in Figure 4) the depth for a given diode on the angle lapped surface is obtained by:

$$d = nx \sin 3^{\circ} \cos \theta$$

where

n = number of a given diode from the surface

x = spacing between the diodes.

Typical spatial resolutions obtained were 3-4 microns although for some samples the resolution was 1 to 2 microns due to a larger angle θ.

The epitaxial layer thicknesses were measured using a split beam microscope. A small piece of the wafer was cleaved before diode fabrication and etched in a 1:1 HF:50% H_2O_2 mixture for 90 seconds under intense illumination along the cleaved edge. Hall measurements were made on the p-layer of the wafers to determine the carrier concentration and compare it with the value previously determined from Schottky Barrier data. The concentration determined from Hall analysis is an average value over the epitaxial layer, whereas C-V analysis gives a concentration for a specific depth in the film. Therefore, generally, we would not expect the two values to coincide.

C. Annealing Procedure

An array containing approximately 15-30 diodes was broken from the GaP wafers. These arrays were annealed in a flow-thru argon system at 400°C and 500°C for times ranging up to 72 hours. A Marshall combustion tube furnace with a 2-3 inch flat zone was used for this purpose. No attempt was made to quench the samples other than the air quench they received because of the low masses and temperatures involved. A 3:1:1 etch (H_2SO_4:30% H_2O_2:H_2O) maintained at 60°C was used to etch the samples after each

annealing cycle[25]. The etch time was 5-10 minutes and the etch rate measured at room temperature is $\approx 0.01 \mu/min$.

Four measurements were made on each sample to characterize the junction and optical properties of the diodes:

1. reverse biased junction capacitance-voltage

2. forward current-voltage characteristics

3. electroluminescent efficiency

4. emission spectra.

These measurements are to be discussed in detail in the following section. Since the measurements were made after each annealing cycle, photographs were used to identify individual diodes so they could be followed throughout the entire experiment.

The experiment could have been conducted with two different approaches: (1) anneal bulk material for different times and then fabricate diodes, or (2) fabricate the diodes prior to annealing the samples. The latter method was chosen because expected changes in junction properties would be small and could be masked by variations between diodes.

D. Measurements

1. Junction Capacitance-Voltage

In 1942 Schottky[26] pointed out that the impurity distribution could be determined from the dependence of the junction capacitance on the junction voltage. The basis for the determination of the

-16-

impurity distribution is the dependence of the variation of the junction depletion width on the concentration of impurities at the edge of the space charge region. The relationship is obtained by a double integration of Poisson's equation:

$$\nabla E(x) = \frac{\rho(x)}{\epsilon} \qquad (1.1)$$

where $E(x)$ is the electric field and $\rho(x)$ is the charge concentration. The assumptions invoked in the analysis are (1) the charge distribution in the space charge region is due only to immobile impurity ions, (2) the impurity atoms are completely ionized, (3) the junction is planar, (4) the applied voltage appears entirely across the junction and (5) that the edges of the space charge layer are well defined.

Applying Poisson's equation in one-dimension:

$$\frac{dE}{dx} = \frac{q}{\epsilon}[p(x) - n(x) + N_D^+(x) - N_A^-(x)] \qquad (1.2)$$

where $p(x)$ is the mobile hole concentration, $n(x)$ is the electron concentration and $N_D^+(x)$ and $N_A^-(x)$ are the ionized donor and acceptor concentrations respectively. Using the depletion approximation that the space charge region is depleted of all mobile carriers equation (1.2) reduces to:

$$\frac{dE}{dx} = \frac{q}{\epsilon}[N_D^+(x) - N_A^-(x)]. \qquad (1.3)$$

In the n-region:

$$\frac{dE}{dx} = \frac{q}{\epsilon} N_D^+(x) \qquad 0 \leq x \leq l_n \qquad (1.4)$$

and in the p-region:

$$\frac{dE}{dx} = - \frac{q}{\epsilon} N_A^-(x) \qquad -l_p \leq x \leq 0 \qquad (1.5)$$

where l_n and l_p are the depletion widths in the n and p regions. Assuming N_D^+ and N_A^- are constant, for ease of manipulation, integration of equations of (1.4) and (1.5) and applying the boundary condition that $E = 0$ at $x = l_n$ and $x = - l_p$, gives:

$$E(x) = + \frac{q N_D^+}{\epsilon} (x - l_n) \qquad 0 \leq x \leq l_n \qquad (1.6)$$

$$E(x) = - \frac{q N_A^-}{\epsilon} (x + l_p) \qquad -l_p \leq x \leq 0 \qquad (1.7)$$

The maximum electric field exists at $x = 0$ and is given by:

$$E_m = - \frac{q N_D^+ l_n}{\epsilon} = - \frac{q N_A^- l_p}{\epsilon} \qquad (1.8)$$

From the above relationship we see that the total ionized immobile impurity in the n-region equals the ionized immobile impurity in

-18-

the p-region. Thus:

$$N_D^+ \, l_n = N_A^- \, l_p \qquad (1.9)$$

Integration of equations (1.6) and (1.7) gives the potential distribution $V(x)$ and the built-in potential V_{bi}:

$$V(x) = E_m \left(x - \frac{x^2}{2l_t} \right) \qquad (1.10)$$

$$V_{bi} = \frac{1}{2} E_m l_t = \frac{1}{2} E_m (l_n + l_p) \qquad (1.11)$$

where l_t is the total depletion width, $l_n + l_p$. From equations (1.8), (1.10) and (1.11)

$$l_t = \left[\frac{2\epsilon}{q} V_{bi} \left(\frac{N_A^- + N_D^+}{N_A^- \cdot N_D^+} \right) \right]^{1/2} \qquad (1.12)$$

Upon application of a voltage V to the junction, the total potential is given by $(V_{bi} + V)$ for reverse bias and $(V_{bi} - V)$ for forward bias.

The depletion layer capacitance is defined as $C \equiv \frac{dQ}{dV}$ where dQ is the incremental increase in charge uncovered upon an incremental change in the applied voltage dV. The total charge Q for a two-sided junction is given by the expression:

$$Q = q N_{eff} l_t . \qquad (1.13)$$

Sze[40] gives the following expression for the differential capacitance of a two-sided step junction:

$$C = \frac{dQ}{dV} = \frac{+d(qN_{eff}l_t)}{d(\frac{q}{2\epsilon}N_{eff}l_t^2)} = \frac{\epsilon}{l_t} \qquad (1.14)$$

$$C = + \left[\frac{q\,\epsilon\,N_{eff}}{2(V_{bi} \overset{+}{\underset{-}{}} V)} \right]^{1/2} \qquad (1.15)$$

where

$$\frac{1}{N_{eff}} = \frac{1}{N_A^-} + \frac{1}{N_D^+} \qquad (1.16)$$

Equation (1.15) can be written:

$$C^2 = + \frac{q\,\epsilon\,N_{eff}}{2(V_{bi} \overset{+}{\underset{-}{}} V)} \qquad (1.17)$$

$$\frac{1}{C^2} = + \frac{2}{q\epsilon} \frac{(V_{bi} \overset{+}{\underset{-}{}} V)}{N_{eff}} \qquad (1.18)$$

Taking the derivative of (1.18)

$$\frac{d(\frac{1}{C^2})}{dV} = \overset{+}{\underset{-}{}} \frac{2}{q\epsilon\,N_{eff}} \qquad (1.19)$$

we see that we can determine the carrier concentration N_{eff} by determining the slope of a plot $\frac{1}{C^2}$ vs V. A straight line

extrapolation of the reverse bias data back to where $\dfrac{1}{C^2} = 0$
gives the built-in potential V_{bi}. The above relationships were
derived assuming that N_A and N_D were constant, although the same
results can be obtained if N_A and N_D are functions of position.

The total depletion width l_t can be determined using the approximation for a parallel-plate capacitor:

$$C = \frac{\epsilon A}{l_t} \, . \tag{1.20}$$

Thus, we know N_{eff} and l_t the total space charge layer thickness
as a function of voltage; however, we wish to determine the concentration of impurities on both sides of the junction. Therefore,
the unknowns are $N_A^-(x)$, $N_D^+(x)$, l_p and l_n. To determine these
values the following relationships are required:

$$l_t = l_p + l_n \tag{1.21}$$

$$N_A^- = \frac{N_{eff} \cdot N_D^+}{N_D^+ - N_{eff}} \tag{1.22}$$

Since we have only two equations but four unknowns another variable
must be known. From Schottky Barrier profiles the impurity concentration, N_D^+, in the Te-doped n-layer can be determined. Assuming
that the diffusion of impurities across the interface during

growth of the p-layer is controlled by the more rapidly diffusing
specie, we can assume that compensation of impurities near the
junction is due only to the fast diffuser. Since $D_{Zn} \approx 10^5 D_{Te}$
at the growth temperature, compensation is attributed to zinc
diffusion. Therefore, the distribution of Te is assumed to follow
a step function at the junction and equals N_D^+ as determined from
Schottky Barrier capacitance measurements.

Figure 5 is a plot of $(\frac{A}{C})^2$ vs V for a 0.07 mole % Zn-doped
GaP diode. The slope of the curve at any point therefore, deter-
mines a value of the effective doping concentration, N_{eff} for a
given voltage or depletion width. Figure 6 is a plot of N_{eff} vs
l_t, the total space charge depletion width, as determined by
using equations (1.19) and (1.20). However, to determine the
values of N_{eff} in the regions of large forward bias, the experi-
mental data shown in Figure 5 was fit with a second order poly-
nomial equation of the form: *

$$y = ax^2 + bx + c$$

where c is the intercept of the voltage axis and was set to the
built-in potential, V_{bi}. N_A^-, l_p and l_n were then calculated
using a numerical iterative technique [27] using equations 1.9,
1.21 and 1.22 as described below.

* A multiple regression program was employed using a least squares
  technique.

-22-

Assuming $N_D^+(T_e)$ is constant in the n-region and N_{eff} vs l_t is known from experimental measurements, $N_A^-(x)$ is calculated on the basis of equal increments of charge on each side of the junction using the following procedure (Figure 7):

(1) $N_A^-(0)$, the net acceptor concentration at the junction, is calculated from $N_{eff}(0)$ and N_D^+ using equation (1.22). $N_{eff}(0)$ is determined from the slope of the polynomial equation where $(\frac{A}{C})^2$ equals zero. At this point $l_t = 0$.

$$N_A^-(0) = \frac{N_D^+ \cdot N_{eff}(0)}{N_D^+ - N_{eff}(0)}$$

(2) $N_A^-(x)$ is assumed constant for a small increment $l_p(1) - l_p(0)$ into the p-region and N_D^+ is constant for a correspondingly small increment $l_n(1) - l_n(0)$ into the n-region so that

$$l_t(1) - l_t(0) = [l_p(1) - l_p(0)] + [l_n(1) - l_n(0)].$$

from equation (1.21).

(3) Since $l_p(1)$ and $l_n(1)$ are both unknown, equation (1.9) can be written in terms of l_p and l_t as follows:

$$N_A^-[l_p(1) - l_p(0)] = N_D^+ \{ [l_t(1) - l_t(0)] - [l_p(1) - l_p(0)] \}$$

or $l_p(1) - l_p(0) = \dfrac{N_D^+[l_t(1) - l_t(0)]}{N_A^- + N_D^+}$

solving for $l_p(1)$ gives

$$l_p(1) = l_p(0) + \dfrac{N_D^+[l_t(1) - l_t(0)]}{N_A^- + N_D^+} \quad \text{and}$$

$$l_n(1) = l_t(1) - l_p(1).$$

(4) $N_A^-(1)$ is then calculated from $N_{eff}(1)$ at $l_t(1)$ and N_D^+ using equation (1.22)

$$N_A^-(1) = \dfrac{N_D^+ \cdot N_{eff}(1)}{N_D^+ - N_{eff}(1)}$$

(5) The sequence of (2) through (4) is repeated until the N_{eff} vs l_t data is exhausted. We have therefore generated the near junction doping profile in the p-layer from N_{eff} data.

2. Current-Voltage Characteristics

The forward current-voltage characteristics were measured at room temperature using a Hewlett-Packard Model 7004A X-Y recorder, thereby providing a continuous plot of the log of the current versus forward voltage. Although the electronics limited the measurement range from 10^{-10} to 10^{-2} amperes, the range was

sufficient since the regions of very low and high currents were
not of interest.

As previously stated the voltage dependence of a p-n junction
in forward bias is given by the expression:

$$I = I_o e^{qV/nkT} \qquad (2.1)$$

where n is a constant dependent on the recombination mechanism.
The value of n in a given region may, therefore, be found by
determining the slope of the log I vs V curve. If

$$I_1 = I_o e^{qV_1/nkT} \qquad \text{and} \qquad (2.2)$$

$$I_2 = I_o e^{qV_2/nkT} \qquad (2.3)$$

then n can be found from the equation:

$$n = \frac{q}{kT} \frac{(V_1 - V_2)}{\ln(I_1/I_2)} \qquad (2.4)$$

In GaP the current-voltage characteristics are dominated by
recombination at deep centers in the space charge region under
medium forward bias. This current component was proposed by Sah,
Noyce and Shockley [28] to explain anomalies in the I-V charac-
teristics of silicon devices and later applied by Morgan [30]
to radiative space-charge recombination. The SNS current compo-
nent for the condition that qV/2kT >> 1 is given by the expression:

$$J_{rg} = \frac{n_i kTW \exp(qV/2kT)}{[\tau_{po}\,\tau_{no}]^{1/2}(V_{bi} - V)} \cdot f(b) \qquad (2.5)$$

where n_i is the intrinsic carrier concentration, W is the voltage dependent space charge width, V_{bi} is the built-in potential and τ_{no} and τ_{po} are the intrinsic electron and hole lifetimes respectively. The function $f(b)$ is a definite integral defined by SNS and approaches $\frac{\pi}{2}$ as a limit for the high bias case and b^{-1} $\ln(b)$ for low bias. The value of b is a function of the trap level, E_t, the intrinsic Fermi level and the intrinsic hole and electron lifetimes. For the case when deep center recombination is dominant equation (2.5) applies and $f(b) = \frac{\pi}{2}$ for medium bias. However, if recombination of hole-electron pairs occurs outside the space charge region, the diffusion current dominates the process and the current voltage relationship takes the form [31]:

$$J_D = \left[\frac{q\,n_{po}D_e}{L_e} + \frac{q\,p_{no}D_h}{L_h}\right] e^{\,qV/kT} \qquad (2.6)$$

where J_D is the diffusion current density in the neutral region and D_e and D_h are diffusion constants for electrons and holes. L_e and L_h are the diffusion lengths defined by $L = \sqrt{D\tau}$ where τ is the lifetime of the carrier. For recombination of hole-electron pairs outside the space charge region, the slope of the I-V curve

must give a value of n = 1; therefore, we can determine the regions of the I-V characteristic dominated by recombination in the space charge layer or neutral region by observing the change in the slope of the curve. Series resistance in the bulk regions of the device dominate the I-V characteristics for voltages greater than approximately 1.80 volts, thus, limiting the analysis to values less than this voltage.

3. Electroluminescent Efficiency

The electroluminescent efficiency of the diodes was measured at room temperature using an integrating sphere. Figure 8 is a schematic illustration of the experimental apparatus. The efficiency test set consists of a reflecting integrating sphere with two silicon solar cell panels located at the top and bottom of the cavity. The absorption filters placed between the cavity and solar cell panels remove light with a wavelength less than 5500 Å. The assembly is enclosed in a light tight black box to reduce the background noise of the solar panels.

The electroluminescent efficiency is the ratio of the number of photons emitted to the number of electrons flowing in the external circuit. For the test set used, the electroluminescent efficiency was determined from the expression:

$$\eta_e = 1.39 \times \frac{V_{Solar\ Cells\ (mv)}}{I\ (ma)} \qquad (3.1)$$

where 1.39 is a correction factor for the test set, V is the output voltage of the solar panels and I is the current flowing in the circuit. The correction factor was obtained by calibration of the test set with a diode of known efficiency.

Contact was made to the diode array by placing the n-side on a gold plated TO-5 can assembly and making a spring contact to the Be-Au contact pad on the p-layer. The measurements were made using a constant dc current of 10 ma. The output voltage of the Si solar cells was measured using a Hewlett-Packard D. C. Null Voltmeter in conjunction with a digital multimeter for a more accurate readout.

4. Emission Spectra

The emission spectra of each sample was measured using a Spex 1800, 3/4 meter monochromator from Czerny Turner Co. The slit width was 2500 microns and the slit height was 5 millimeters. The measurements were made in the 6,000 Å – 10,000 Å range in 50 Å increments. For all measurements, the diodes were driven with a constant current of 10 ma as in the efficiency measurements.

An ITT FW 130 photomultiplier tube was used in conjunction with a photon counting system to detect the light intensity emitted from the diodes. The useful range of the photomultiplier tube extends beyond the 6,000 Å – 10,000 Å range used in the experiment.

The sample diode was placed directly in front of the slit to the monochromator. A sharp cut Corning #CS 3-69 filter was used in conjunction with a #CS 3-76 filter to remove any light with a wavelength less than 5500 Å. The raw data was recorded on magnetic tape using a data acquisition system as previously described.

Using the algorithm of Dishman, DiDomenico and Caruso [9], the value of the integrated red-to-infrared intensity ratio may be calculated. For the purpose of calculating the ratio the alogrithm is used to express the area of the red and infrared bands in terms of their peak heights. Thus, if P_r and P_{ir} are the values of the maxima of the red and infrared bands, then the room temperature quantum efficiencies are given by:

$$\eta_r = 0.263 \; P_r \tag{4.1}$$

$$\eta_{ir} = 0.236 \; (P_{ir} - 0.0135 \; P_r) \tag{4.2}$$

Therefore, the integrated red-to-infrared ratio can be determined by dividing equation (4.1) by (4.2).

$$\text{RED/IR RATIO} = \frac{0.263 \; P_r}{0.236 \; (P_{ir} - 0.0135 \; P_r)} \tag{4.3}$$

E. Ion Microprobe Sample Preparation

To check the validity of the assumption made in the capacitance-voltage section; i.e., that the Te profile is constant throughout the n-layer, and also to provide a second method for determining the zinc concentration in the p-layer it was decided to profile bulk epitaxial layers using an ion microprobe. The ion microprobe was chosen over the electron microprobe because of its much greater sensitivity, parts per billion compared to parts per million for the electron microprobe. The increased sensitivity is the result of analyzing secondary ions with a mass spectrometer and not secondary electrons as with the electron probe. Since the maximum concentration of impurities in the epitaxial layers is on the order of 1×10^{18} cm^{-3}, these levels lie outside the resolution of the electron microprobe.

The samples were diffused at 400°, 500°, 700° and 800°C for times ranging from 1 to 120 hours in nitrogen. The impurity species of interest in the epitaxial layers are Zn and Te. Since the layers are relatively thick 35-40 microns, the samples were angle lapped so concentration profiles could be determined along the lapped surface. The specimens were lapped at 3° on a glass plate using a 3 micron diamond compound. The samples were then polished on a nylon polishing cloth using 1 micron and 1/4 micron diamond polish. The samples were degreased in trichlorethylene,

acetone and methanol and then etched for 10 seconds in chlorine saturated methanol to remove damage introduced in the polishing operation.

The specimens were mounted on 3° aluminum wedges so that the lapped surface would be normal to the ion beam when loaded into the specimen chamber of the probe. The ion microprobe analysis was conducted at Cameca Instruments in Elmsford, New York.

III. RESULTS

The resistivity, hole mobility and carrier concentration in the p-layer, measured by standard techniques, is tabulated in Table I. Impurity profiles of three epitaxial wafers from which diodes were fabricated are shown in Figures 9, 10 and 11 for two different zinc concentrations. The concentration profiles were determined by making a series of C-V measurements on evaporated metal-semiconductor Schottky Barrier diodes.

Figures 12 and 13 are plots of the electroluminescent efficiency versus annealing time for annealing temperatures of $400^{\circ}C$ and $500^{\circ}C$ respectively. The data points represent the average efficiency for diodes of a given zinc concentration, determined from Schottky Barrier measurements, found in Tables II and III. Figure 14 shows the effect of zinc concentration on the maximum electroluminescent efficiency. Again the data points represent the average efficiency for an annealing time of 50 hours. Typical emission spectra for unannealed and annealed diodes for two zinc concentrations are shown in Figures 15, 16, 17 and 18. Plots of the average integrated Red-to-Infrared Ratio versus annealing time are shown in Figures 19 and 20. Tabulation of the integrated Red-to-Infrared Ratio can be found in Tables IV and V.

Figure 6 is a plot of N_{eff} versus total depletion width,

l_t, showing the effect of the zinc concentration on the near junction impurity profile for a constant Ga_2O_3 concentration and Te concentration. Typical plots of $(\frac{A}{C})^2$ versus voltage are shown in Figures 21 and 22 for the two zinc doping levels investigated. The figures also display the effects of annealing on the junction characteristics by plotting the initial C-V characteristics and the characteristics at some period of time in the annealing cycle. Figures 26 and 27 are plots of the acceptor doping profile determined using the numerical iterative technique. Figure 30 summarizes the results obtained from C-V analysis by plotting the diffusion coefficient of zinc versus the zinc concentration.

The current-voltage characteristics of typical unannealed GaP diodes are shown in Figure 31. The I-V characteristics for annealed diodes are exhibited in Figures 32 and 33 and compared to the unannealed curves.

IV. DISCUSSION OF RESULTS

A. General

The n-epitaxial layer thickness measured using a split beam microscope ranged between 1.17 and 1.86 mils. Difficulty was encountered in determining the thickness of the n-layer in some samples due to the graded interface between the epitaxial layer and the selenium doped n-type substrate. The p-layer epitaxial thickness was measured using the above technique and was found to vary from 1.58 to 1.93 mils.

The hole mobility and average carrier concentration in the Zn,0 doped p-layer was determined from Hall measurements. Mobilities ranged from 81.6 cm^2/volt-sec in the heavily doped material to 94.5 cm^2/volt-sec in the more lightly doped layers. Average carrier concentrations varied from 5.95-7.02 x 10^{17} cm^{-3} for the 0.07 mole % Zn doped layers to 3.43-4.70 x 10^{17} cm^{-3} for the 0.04 mole % Zn doped samples. Comparison of the concentrations determined from Hall analysis with Schottky Barrier data shows that the concentration determined from Hall measurements is lower in all the samples; however, agreement is generally good to within a factor less than two. Since Hall measurements provide an average concentration for the entire layer, concentration variations throughout the layer are not observed; therefore,

Schottky Barrier capacitance measurements provide a more meaningful insight into doping profiles since they allow a spatial analysis of the layer to be made. Logan et al.[21] reported agreement within 15-20% for Hall and Schottky Barrier measurements; however, concentrations were determined in bulk samples and not epitaxial layers.

B. Electroluminescent Efficiency

As seen in Figures 12 and 13 annealing at $400^{\circ}C$ and $500^{\circ}C$ increases the external quantum efficiency as has been previously reported. The efficiency being measured using the integrating sphere is the total quantum efficiency; i.e., the sum of the red and infrared efficiencies. Figure 12 shows that the electroluminescent efficiency increases slowly with annealing time at $400^{\circ}C$ and doesn't reach a maximum until 48 to 72 hours have elapsed. The increase in the efficiency with annealing time is about a factor of two. A parameter that has a considerable influence on the efficiency of the diodes is the zinc concentration in the p-layer. For all of the diodes tested, the Ga_2O_3 concentration in the p-layer was held constant while the zinc concentration was varied. As can be seen in Figure 12 the higher zinc concentrations resulted in lower electroluminescent efficiencies both before and during annealing. The peak efficiency for the heavily doped p-layer, 1.1×10^{-18} cm^{-3}, is reached in approximately 16 hours while 3 to 4 times as long is

required for the more lightly doped material to reach its maximum. However, the maximum efficiency attained in the heavily doped material is only about one-half the efficiency of the more lightly doped samples.

The efficiency data for the $500^{\circ}C$ annealed diodes (Figure 13) exhibit the same general characteristics as the $400^{\circ}C$ annealed diodes. The increase in efficiency with annealing is a factor of 2-1/2 to 3 as compared to 2 for the lower temperature. At the higher temperature the peak efficiency is reached at a much shorter time than for the $400^{\circ}C$ anneal. Once again a strong concentration dependence of the electroluminescent efficiency is displayed.

Figure 14 summarizes the efficiency data for the two annealing conditions by plotting the maximum efficiency as a function of the log of the zinc concentration. The data exhibits a strong dependence of efficiency on zinc concentration for a constant Ga_2O_3 concentration. Such a dependence has been previously reported by Saul, Armstrong and Hackett[32] for p on n LPE diodes. At some zinc concentration it would be expected that the electroluminescent efficiency would decrease with decreasing zinc concentrations; however, this was not observed for the concentration range investigated.

Since the integrating sphere measures the total red plus infrared external quantum efficiency, from efficiency measurements alone we can not tell if the red efficiency, infrared efficiency or both

are increasing or decreasing with annealing. However, from knowledge of the emission spectra to be discussed in the following section, approximately 98% of the emitted light is in the red band; therefore, the increase in the total efficiency is due to formation of Zn-O complexes during annealing.

C. Emission Spectra

It may be seen from the normalized emission spectra for unannealed and annealed diodes shown in Figures 15 through 18, that the room temperature spectra is composed of a red band centered at approximately 7000 $\overset{\circ}{A}$ and an infrared band at 9200 $\overset{\circ}{A}$. At room temperature these two bands overlap each other. The red band is associated with excitonic recombination at Zn-O nearest neighbor pairs while the infrared emission is associated with unpaired oxygen on substitutional lattice sites. As can be seen from these emission spectra, the area of the infrared band decreases relative to the red band for annealed diodes. Also the area in the infrared region of the spectrum for the 0.07 mole % Zn doped diodes is less than that for the 0.04 mole % Zn doped diodes. This implies that a larger percentage of the substitutional oxygen is paired with Zn forming Zn-O complexes resulting in a larger red band compared to the infrared band for the more heavily doped diodes.

The change in the integrated red-to-infrared ratio with annealing time, shown in Figures 19 and 20, shows that annealing

increases the emission intensity ratio for the temperatures inves-
tigated. At 400°C the intensity ratio increases slowly with an-
nealing time for $4.5 - 5.5 \times 10^{17}$ cm^{-3} concentration range and
doesn't approach an equilibrium value until approximately 72 hours
have elapsed. Even at 72 hours the ratio is slowly increasing;
however, it seems to be approaching a plateau. The heavily doped
diodes (1.1×10^{18} cm^{-3}) increased rapidly with time and reached
a plateau in approximately 12 to 16 hours. The change in the
intensity ratio is about three for all concentrations. At 500°C
the increase in the intensity ratio occurs more rapidly than at
400°C and reaches an equilibrium plateau in approximately 24 hours.
The increase in the intensity ratio is about four at 500°C. The
behavior of the heavily doped diodes is very erratic at both temper-
atures and cannot be explained; therefore, the dotted curves in the
figures are the expected values and shape of the data.

The intensity ratio exhibits a strong dependence on the doping
concentration in the p-layer. Wiley[33] has shown that for a known
oxygen concentration and annealing temperature, the equilibrium
fraction of paired oxygen to total substitutional oxygen increases
with the zinc concentration. Therefore the concentration of Zn-O
complexes increases with increasing Zn concentration resulting in
an increase of the integrated red-to-infrared ratio. The equilibrium
pairing fraction increases with decreasing temperature for a known

zinc and oxygen concentration.

The 400°C emission data follows Wiley's model since the intensity ratio decreases with decreasing zinc concentration. The 500°C data also fits the model except that the 4.5×10^{17} cm^{-3} doped samples give a slightly higher value than the 5.5×10^{17} cm^{-3} doped samples. However, the concentrations are bulk concentrations; i.e., determined approximately 3 to 5 microns from the p-n junction, therefore the near junction zinc concentration needs to be determined. It has been shown that the red emission occurs within approximately 1 to 2 microns of the space charge region on the p-side[34]; therefore, the deviation from Wiley's model could be due to the variations in the near junction doping profiles between the diodes. Since the intensity ratio at 500°C is greater than at 400°C, the discrepancy could be due to the effects of p-n junction properties on the emission spectra.

D. Capacitance-Voltage Measurements

The electroluminescent efficiency of GaP diodes is not only a function of the bulk properties of the p-layer, but also a function of the junction properties of the device. Since red luminescence occurs by radiative recombination of injected electrons at Zn-O complexes in the p-layer, the near junction doping concentrations and the lifetime of the injected electrons are important parameters to be characterized. The injection efficiency, γ, is defined by the relation:

$$\gamma = \frac{J_e}{J_e + J_h}$$

where J_e and J_h are the electron and hole components of the current density flowing across the p-n junction. In forward bias J_e and J_h are proportional to the gradient of the electron and hole concentrations near the junction; therefore, the near junction doping profiles are required if the effects of injection efficiency on the luminescent properties are to be investigated.

Because of the high diffusivity of Zn in GaP, diffusion of Zn into the n-epitaxial layer during growth of the p-layer and subsequent heat treatment results in a compensated region separating the active p-region from the n-region. A close approximation of the junction doping profile can be discerned from the N_{eff} vs. 1_t data. The width of the compensated region in the p-π-n structure is

important since electron injection into the p-region is limited by the number of electrons that recombine non-radiatively in this region.

From the plot of $(\frac{A}{C})^2$ versus voltage in Figure 5, it is deduced that the diode junctions are step junctions separated by an intrinsic π- layer. The p-π-n structure explains the large voltage intercept obtained by a straight line extrapolation of the reverse bias data. For a simple p-n structure in GaP without a π-layer, the voltage intercept is ≈ 2.0 volts, the built-in voltage, V_{bi}. Deviations from the straight line extrapolation in the forward bias region have been explained to be due to the presence of deep states in the energy gap[29]. Also to be considered in the region of large forward bias is the effect of diffusion capacitance due to the storage of a large number of minority carriers near the edges of the space charge region.

Figures 21 and 22 are plots of $(\frac{A}{C})^2$ versus voltage for typical diodes doped with 0.07 mole % and 0.04 mole % zinc. The data shown is for the unannealed condition and at a later time in the annealing cycle. By drawing a straight line parallel to the reverse bias data for the unannealed case with an intercept value of $V_{bi} = 2.0$ volts, the width of the intrinsic layer can be determined from the relation:

$$W = \epsilon A \left[\frac{1}{c_2^2} - \frac{1}{c_1^2} \right]^{1/2}$$

-41-

where C_1 is the zero bias capacitance for the simple p-n junction and C_2 is the zero bias capacitance for the p-π-n structure. Calculations of the π-layer width for unannealed diodes resulted in widths of ≈ 800 Å for the 0.07 mole % material and ≈ 250 Å for the 0.04 mole % Zn-doped material. Annealing at 400°C for 16 hours results in a change in the slope of $(\frac{A}{C})^2$ versus V data and an increase in the width of the compensated π-layer from 800 Å to ≈ 900 Å.

Figure 6 is a plot of the effective carrier concentration, N_{eff}, versus total space charge width, 1_t, obtained by determining the slope of the $(\frac{A}{C})^2$ vs. V curve. The two curves show the effect of the zinc concentration on the effective doping profile near the junction. The curve for the 0.07 mole % Zn-doped diode displays a much steeper gradient than for the more lightly doped 0.04 mole% diode. Also, the concentration near the junction is _less_ than in the lightly doped material. From Schottky Barrier capacitance measurements, the net acceptor concentration measured ≈ 5 microns from the junction was $\approx 1.1 \times 10^{18}$ cm^{-3} for the 0.07 mole % material and 5.5×10^{17} cm^{-3} for the 0.04 mole % material. From these measurements N_{eff} for the heavily doped diode would be expected to be higher than for the more lightly doped diode. However, the diffusion coefficient of zinc in GaP is known to be a strong function of the zinc concentration at the temperatures where

where C_1 is the zero bias capacitance for the simple p-n junction and C_2 is the zero bias capacitance for the p-π-n structure. Calculations of the π-layer width for unannealed diodes resulted in widths of ≈ 800 Å for the 0.07 mole % material and ≈ 250 Å for the 0.04 mole % Zn-doped material. Annealing at 400°C for 16 hours results in a change in the slope of $(\frac{A}{C})^2$ versus V data and an increase in the width of the compensated π-layer from 800 Å to ≈ 900 Å.

Figure 6 is a plot of the effective carrier concentration, N_{eff}, versus total space charge width, l_t, obtained by determining the slope of the $(\frac{A}{C})^2$ vs. V curve. The two curves show the effect of the zinc concentration on the effective doping profile near the junction. The curve for the 0.07 mole % Zn-doped diode displays a much steeper gradient than for the more lightly doped 0.04 mole% diode. Also, the concentration near the junction is less than in the lightly doped material. From Schottky Barrier capacitance measurements, the net acceptor concentration measured ≈ 5 microns from the junction was $\approx 1.1 \times 10^{18}$ cm^{-3} for the 0.07 mole % material and 5.5×10^{17} cm^{-3} for the 0.04 mole % material. From these measurements N_{eff} for the heavily doped diode would be expected to be higher than for the more lightly doped diode. However, the diffusion coefficient of zinc in GaP is known to be a strong function of the zinc concentration at the temperatures where

epitaxial growth occurs. Chang and Pearson[14] have shown that the dependence of D_{Zn} follows a square law dependence of the zinc concentration at the growth temperature. Imposing this dependence of the diffusion coefficient could explain the difference in the near junction effective concentration profiles. Because of the high D_{Zn} for the 0.07 mole % diodes, rapid zinc diffusion across the p-n junction during growth results in compensation of the tellurium donor atoms. This compensation reduces the net donor concentration in the n-region resulting in a smaller value of N_{eff}.

The results of annealing at $400^{\circ}C$ and $500^{\circ}C$ on the effective doping concentration are shown in Figures 23 and 24 as a function of annealing time. The two diodes represent typical diodes for the 0.07 mole % doping level. Data for the 0.04 mole % diodes is not shown since problems were encountered in obtaining a good fit of the experimental capacitance-voltage data in the forward bias region. The fit to the experimental data with a second order polynomial was extremely good in both the forward bias and reverse bias regions for the 0.07 mole % diodes.

From the plots of N_{eff} vs. l_t, the gradient of the effective concentration is shallow near the junction ($l_t = 0$) and increases with increasing depletion depth into the material. The region of the curve displaying a relatively constant value of N_{eff} is the region in which compensation of impurities occur during epitaxial

growth. Subsequent heat treatment at 400°C and 500°C reduces the concentration gradient and increases the width of the π-layer. Although N_{eff} vs. l_t data shows that diffusion of impurities across the p-n junction occurs during low temperature annealing, a direct knowledge of the impurity distribution in both the n and p layers as a function of time would be beneficial in understanding how diffusion affects the diode injection efficiency. Also, the diffusion coefficient of Zn could be determined by knowing $N_A^-(x)$ as a function of time and temperature.

Figure 25 is a plot of the calculated doping profile in the n and p regions near the p-n junction obtained from N_{eff} vs. l_t data using the numerical iterative technique. The plot shows the distribution of impurities after epitaxial growth and before any subsequent heat treatments have occurred. In the numerical analysis it was assumed that the tellurium concentration (N_D^+) in the n-layer was constant and that compensation of impurities near the junction was due to zinc migration because of its much higher diffusivity. In the flat region of the curve to the right of the n-π interface, compensation has occurred and the material is weakly p-type for ≈ 0.1 microns into the p-layer. To the right of the π-p interface, the acceptor concentration rises rapidly and reaches a value of $\approx 6.5 \times 10^{17}$ cm^{-3} at 0.23 microns. The acceptor concentration, N_A^-, should approach the value of 1.1×10^{18} cm^{-3} determined from

Schottky Barrier analysis of the p-layer.

Figures 26 and 27 show the effects of low temperature annealing on the acceptor concentration for temperatures of $400^{\circ}C$ and $500^{\circ}C$. The gradient of the concentration decreases with annealing time for a given temperature, thus verifying that zinc is out-diffusing from the p-layer across the junction. Figures 28 and 29 are plots of l_p vs. $\sqrt{t}$ for a given acceptor concentration N_A^-. For increasing values of N_A^-, the slope of the l_p vs. $\sqrt{t}$ curve increases for a given temperature implying that D_{Zn} is concentration dependent as observed by Chang and Pearson[12-14]. Also the slope of the curves in Figure 29 for a temperature of $500^{\circ}C$ is larger at a given N_A^- than at a temperature of $400^{\circ}C$. Assuming that D_{Zn} is constant over a small concentration range and that diffusion occurs from an infinite source, an approximate value of D_{Zn} can be obtained from the expression:

$$l_p = 2\sqrt{D_{Zn}t}$$

where $2\sqrt{D_{Zn}}$ is the slope of the line. Plotting the calculated values of $\log(D_{Zn})$ vs. $\log(C_{Zn})$ in Figure 30, the concentration dependence of D_{Zn} can be observed. Also shown are the values predicted by Chang and Pearson from their low temperature data. They predicted a dependence of $C_{Zn}^{0.45}$ for temperatures less than $900^{\circ}C$; however, the lowest temperature measured was $800^{\circ}C$. The present

-45-

data, both at 400°C and 500°C are within an order of magnitude agreement with the work of Chang and Pearson. The slope of the 500°C curve gives a concentration dependence of $C_{Zn}^{0.70}$ and is in good agreement with previous results. The 400°C data should be expected to show similar results. The low value at 3×10^{17} cm^{-3} is therefore either thought to be in error or is low due to the errors involved in the approximate method used to calculate D_{Zn}.

The discrepancy between the values calculated from C-V analysis and those determined by Chang and Pearson can be possibly explained by the following arguments: (1) extrapolation of Chang and Pearsons data to temperatures of 500°C or less is not valid, (2) the diffusion coefficient of zinc determined by the C-V technique contains a field-aided component due to the electric field across the p-n junction [36], and (3) the method used to determine D_{Zn} is invalid since $D_{Zn} = f(C_{Zn})$.

To determine an expression for D_{Zn} as a function of concentration and temperature would require a more involved analysis. A Boltzmann-Matano analysis cannot be employed since the spatial dependence of the zinc concentration is known only in the concentration range greater than $\approx 1.0 \times 10^{17}$ cm^{-3} and not for all ranges in concentration. However, using a forward finite difference technique similar to that described by von Rosenberg[37] an expression for D_{Zn} could be determined by numerical analysis using a digital computer.

Since N_A^- vs. l_p data is known as a function of both time and temperature, functionalities of D_{Zn} could be assumed and concentration profiles calculated using the assumed values of D_{Zn}. Those D_{Zn} values that produce calculated profiles matching the profiles obtained from junction C-V measurements would then correspond to the diffusion coefficient of zinc at a given concentration and temperature.

E. Current-Voltage Characteristics

The diode current is plotted logarithmically against the forward bias voltage at room temperature in Figure 31 for two typical diodes. The lower curve represents a diode with a 1.1×10^{18} cm^{-3} Zn concentration while the upper curve represents a typical diode with a 5.5×10^{17} cm^{-3} Zn concentration. The curves can be approximated by a series of straight lines in the bias range covered, implying that the current is related to the voltage by the expression $I = I_o \exp(AV)$ where A is a constant for each range. Thermal injection currents vary as $\exp(qV/nkT)$ where q is the electronic charge, k is the Boltzmann factor, T is the absolute temperature and n is a parameter for each region that is temperature independent. The allowed n values lie between 1 and 2 and are dependent on the recombination mechanism.

The apparent increase of n to values greater than 2 as shown in Figure 31 for an unannealed diode is due to an excess current component. Typical currents of Zn,O doped GaP diodes range from approximately 1×10^{-8} to 2×10^{-7} amperes at 1.4 volts. Thus the current for diode 450-16B1 is approximately 1 to 2 orders of magnitude higher than expected.

Normal fabrication procedure for Zn,O doped GaP diodes is to etch the diodes in a 3:1:1 solution, previously described, maintained at 60°C for 5 minutes to remove the surface damage from the dicing

operation. The etching is performed after the diodes have been mounted on TO-18 headers and lead bonded. Used in the prescribed manner, the etch removes about 8 microns of material from the edge of the chip. Hackett et al.[38] have observed from scanning electron micrographs that the 3:1:1 solution etches the p-layer preferentially producing an etch step at the junction for diodes bonded on headers. However, for unmounted diodes the etch step is not present and thus the damaged layer has not been removed. Since diodes used in this investigation were not bonded on headers, the high excess current could be possibly attributed to incomplete removal of the damaged layer. The dicing operation introduces deep states in the energy gap; therefore, the excess current should vary as $\exp(qV/2kT)$, the same as the SNS current component, and thus will result in an upward translation of the "true" I-V characteristics.

Inspection of the diodes used in this investigation at 200X failed to reveal the etch step; therefore, five diodes from each wafer were mounted on headers and lead bonded. The specimens were etched in the 3:1:1 solution at $60^{\circ}C$ for 10 minutes to insure removal of the damaged layer. Visual inspection at 200X revealed the etch step previously reported. Current-voltage characteristics reveal that the current at 1.4 volts is only approximately a factor of 2 to 4 less than for the unbonded diodes and a few resulted in equal or higher currents at this bias. Reductions in the current

level of a factor of ≈ 10 occurred at lower biases (1.0 - 1.2 volts). Since the excess current component was not reduced by a large factor and is still quite large, on the order of microamperes for some diodes, it is deduced that the excess current is not due to incomplete removal of the damaged layer.

To account for values of n > 2 Kleinman[39] ascribed the effect to nonlinear recombination of carriers while Logan et al.[16] have reported that the excess current is due to a tunneling mechanism. However, it is believed by the author that the excess current is due to poor junction fabrication during epitaxial growth.

In Figure 31 the I-V characteristic of diode 443-45B1 is dominated by the SNS space charge recombination component (n $\approx$ 2) in the bias range from 1.1 to 1.6 volts and a parallel mode recombination mechanism between 1.6 and 1.75 volts. The parallel mode recombination (1 < n < 2) is the result of the effects of space charge recombination and diffusion current recombination both being active. For voltages greater than 1.75 volts the I-V characteristic is dominated by series resistance in the bulk regions of the device. Diode 450-16B1 is dominated by the excess current up to about 1.6 volts where the space charge recombination term becomes dominant.

The Shockley-Read lifetime $[\tau_{po} \tau_{no}]^{1/2}$ can be calculated by using equation (2.5) and assuming a value of V_{bi} = 2.0 volts and n_i = 1.5 cm^{-3*} at 300°K. The value of W, the voltage dependent space

* Remember that the energy gap, E_g, in GaP is $\approx$ 2.26 ev at 27°C.

-50-

charge width, is calculated from the C-V characteristics at 1.6 volts using equation (1.20). The calculated values of $[\tau_{po} \tau_{no}]^{1/2}$ for diodes 443-45B1 and 450-16B1 at 1.6 volts are 2.24×10^{-10} sec. and 8.33×10^{-11} sec. respectively.

Figure 32 is a plot of the I-V characteristics of diode 443-45B1 in an unannealed condition and after 12 hours at $400°C$. Throughout the voltage range of 1.1 to 1.6 volts there is a significant reduction in the current attributed to annihilation of recombination centers in the space charge region. After annealing the slope of the curve in this region is the same as for the unannealed condition (n = 1.92); however, at higher bias the n value has decreased from 1.45 to 1.33 implying that the space charge recombination current component is becoming less important. Thus the carrier lifetime increases since fewer injected electrons recombine in the space charge layer. This increase in lifetime benefits the red luminescence process since more carriers are available for excitonic recombination at Zn-O complexes in the p-layer. The Shockley-Read lifetime determined at 1.6 volts for the annealed diode is 3.16×10^{-10} sec., thus annealing increased the lifetime by a factor of ≈ 1.4. Figure 33 shows the effect of annealing at $500°C$ on the I-V characteristics for 12 hours. The current is decreased at a given voltage as also seen at $400°C$. The lifetime is increased by a factor of ≈ 4 by annealing at $500°C$.

F. Ion Microprobe

The absolute concentration of Zn in GaP using the ion micro-
probe could not be determined since a suitable standard is not
presently available. The ion yield, the ratio of ions collected in
the mass spectrometer to the number of generated ions, has a strong
dependence on the matrix; therefore, the standard and specimen must
be of the same matrix material to eliminate this effect. However,
relative concentrations can generally be easily determined. In
analyzing the samples the Zn peak located at a mass-to-charge (m/e)
ratio of 64 was measured relative to a PO_2 peak located at a m/e
ratio of 63. However, in GaP the tail of the large Ga peak at a
m/e ratio of 69 swamps out the Zn 64 peak. Therefore, this tech-
nique of determining the Zn concentration could not be used. Instead
of looking at Zn^+ ions it was decided to look at ZnO^- ions located
at m/e ratios of 80, 82, 83 and 84 to see if the peaks are dis-
tinguishable. Preliminary results reveal that this technique can
reveal the peaks and has potential for making concentration profiles
of Zn in GaP.

A mass spectrum of the p-epitaxial layer and the n-type sub-
strate revealed that the p-layer was relatively clean of foreign
impurities although traces of Al, Na and K were present; however,
the substrate material contained very large quantities of C, Na,
Al, Si, K and other elements. From these results it is concluded

that quantitative evaluation of doping profiles by the ion probe
method could only be accomplished on specially prepared high purity
substrates and that the magnitude of the Zn concentration should be
1 to 2 orders higher than was available in the material investigated.

V. CONCLUSIONS

1. The electroluminscent efficiency of the diodes increases about a factor of 2 to 3 with annealing at 400°C and 500°C. The 500°C anneal gave slightly higher efficiencies than at 400°C.

2. The electroluminescent efficiency of unannealed and annealed diodes has a strong dependence on the zinc concentration in the p-layer for a constant Ga_2O_3 and Te concentration. The lower zinc concentration diodes, 0.04 mole %, had about twice the efficiency as the 0.07 mole % diodes.

3. Annealing at 400°C and 500°C increases the integrated Red/Infrared ratio due to formation of Zn, O pairs on nearest neighbor sites. The 500°C anneal gave higher Red/Infrared ratios than 400°C, in disagreement with Wiley's model for Zn, O pairing. However, the discrepancy can be attributed to the difference between bulk material and material containing a junction.

4. The Red/Infrared ratio is concentration dependent with the higher Zn concentration providing larger intensity ratios due to formation of more Zn-O complexes.

5. Space charge recombination dominates the I-V characteristics of GaP diodes for voltages less than 1.6 volts. A parallel mode recombination mechanism dominates the characteristics for voltages greater than 1.6 volts.

6. Annealing decreases the current of all bias levels and can be attributed to annihilation of recombination centers in the space charge region. The annihilation is seen by an increase in the Shockley-Read lifetime $[\tau_{po}\tau_{no}]^{1/2}$.

7. Zinc diffusion across the p-n junction during low temperature annealing is directly observed by the change in gradient of the acceptor concentration with annealing time. From junction C-V measurements the diffusion coefficient, D_{Zn}, was found to be concentration dependent and varied as $C_{Zn}^{0.70}$ at $500^{\circ}C$.

8. Although some junction degradation did occur, sufficient amounts were not observed to have serious effects on quantum efficiency of the diodes; therefore, it is concluded that pairing of Zn and O in the p-region during annealing more than offsets any degradation effects.

TABLE I

RESISTIVITY, MOBILITY AND CARRIER CONCENTRATION

IN P-EPITAXIAL LAYER DETERMINED BY HALL ANALYSIS

Wafer Number	Zinc Conc. In Melt (Mole %)	N-Epi Thickness (Mils)	P-Epi Thickness (Mils)	Resistivity P-Layer (ohm-cm)	Hole Mobility (cm^2/volt-sec)	Carrier Conc. P-Layer (cm^{-3})
443-45	0.07	1.17	1.61	0.109	81.6	7.02×10^{17}
448-54	0.07		1.58	0.114	85.3	6.43×10^{17}
450-55	0.07	1.63	1.93	0.125	84.2	5.95×10^{17}
450-16	0.04	1.29	1.73	0.193	94.5	3.43×10^{17}
450-17	0.04		1.77	0.165	92.5	4.09×10^{17}
450-18	0.04	1.30	1.71	0.146	91.4	4.70×10^{17}
450-20	0.04	1.86	1.84	0.159	86.9	4.51×10^{17}

Ga_2O_3 Conc. In Melt: 0.07 Mole %

TABLE II

ELECTROLUMINESCENT EFFICIENCY DATA

ANNEALING TEMPERATURE: 400°C

Diode	ANNEALING TIME (HOURS)								
	0	4	8	12	16	24	32	50	72
44345B-1	0.154	0.126	0.149	0.176	0.215	0.223	0.228	0.246	
-2	0.138	0.125	0.148	0.179	0.209	0.232	0.234	0.244	
-3	0.142	0.132	0.156	0.188	0.219	0.236	0.239	0.252	
-4	0.136	0.128	0.150	0.181	0.210	0.227	0.230	0.242	
44345C-1	0.136	0.126	0.161	0.197	0.229	0.245	0.260	0.274	0.244
-2	0.131	0.120	0.161	0.209	0.250	0.277	0.286	0.308	
-3	0.141	0.129	0.174	0.219	0.248	0.277	0.284	0.283	
-4	0.143	0.127	0.171	0.211	0.246	0.273	0.281	0.289	
Average	0.140	0.127	0.159	0.195	0.228	0.249	0.255	0.267	
45016B-1	0.258	0.263	0.276	0.312	0.350	0.411	0.467	0.588	
-2	0.250	0.256	0.280	0.316	0.342	0.407	0.449	0.579	
-3	0.238	0.241	0.255	0.282	0.294	0.367	0.410	0.522	
-4	0.274	0.281	0.297	0.328	0.354	0.416	0.475	0.593	
45016C-1	0.204	0.203	0.213	0.246	0.274	0.325	0.372	0.438	0.437
-2	0.216	0.216	0.222	0.249	0.280	0.345	0.406	0.460	
-3	0.219	0.217	0.226	0.252	0.290	0.355	0.386	0.455	0.439
-4	0.230	0.221	0.239	0.270	0.303	0.362	0.402	0.476	0.462
Average	0.236	0.237	0.251	0.282	0.311	0.374	0.421	0.514	0.446
45018B-1	0.263	0.283	0.295	0.337	0.343	0.407	0.465	0.568	0.539
-2	0.236	0.259	0.261	0.303	0.300	0.384	0.432	0.532	0.519
-3	0.329	0.358	0.374	0.414	0.469	0.554	0.595	0.684	0.675
-4	0.330	0.348	0.349	0.387	0.433	0.512	0.541	0.649	0.618
Average	0.290	0.312	0.320	0.360	0.386	0.464	0.508	0.608	0.588

TABLE III

ELECTROLUMINESCENT EFFICIENCY DATA

ANNEALING TEMPERATURE: 500°C

Diode	ANNEALING TIME (HOURS)								
	0	2	4	8	12	16	24	32	50
44345A-1	0.114	0.229	0.285	0.317	0.298	0.309	0.311	0.266	0.296
-2	0.115	0.218	0.286	0.305	0.289	0.298	0.309	0.271	0.319
-3	0.112	0.210	0.278	0.277	0.281	0.294	0.314	0.282	0.324
-4	0.116	0.233	0.294	0.296	0.299	0.316	0.325	0.286	0.293
-5	0.117	0.234	0.289	0.316	0.306	0.312	0.307	0.287	0.324
Average	0.115	0.225	0.286	0.302	0.295	0.306	0.313	0.278	0.311
45016A-1	0.234	0.339	0.441	0.509	0.528	0.428	0.570	0.513	0.618
-2	0.207	0.295	0.382	0.410	0.447	0.469	0.470	0.442	0.533
-3	0.229	0.367	0.476	0.524	0.552	0.545	0.608	0.544	0.604
-4	0.216	0.327	0.427	0.483	0.507	0.548	0.574	0.528	0.517
-5	0.220	0.339	0.437	0.494	0.502	0.532	0.525	0.500	0.562
Average	0.221	0.333	0.433	0.484	0.507	0.504	0.549	0.505	0.567
45018A-1	0.265	0.379	0.484	0.549	0.591	0.554	0.651	0.598	0.676
-2	0.277	0.435	0.561	0.611	0.640	0.630	0.697	0.660	0.697
-3	0.188	0.318	0.424	0.475	0.496	0.521	0.576	0.542	0.558
-4	0.253	0.360	0.475	0.504	0.540	0.567	0.608	0.500	0.630
-5	0.274	0.395	0.494	0.563	0.595	0.598	0.662	0.641	0.691
Average	0.251	0.377	0.488	0.540	0.572	0.574	0.639	0.588	0.650

TABLE IV

SPECTRAL INTENSITY DATA

ANNEALING TEMPERATURE: 400°C

INTEGRATED RED-TO-INFRARED RATIO

Diode	ANNEALING TIME (HOURS)								
	0	4	8	12	16	24	32	50	72
44345B-1	29.1	36.4	73.0	61.5	113.4	62.2	67.4	53.3	
-2	25.5	36.6	69.6	72.2	105.8	84.1	77.9	57.0	
-3	24.4	35.4	69.9	69.0	78.6	69.7	64.7	54.1	
-4	26.6	36.7	59.8	76.1	81.5	101.2	62.1	57.5	
44345C-1	26.2	35.8	76.1	73.2	98.8	83.3	91.1	80.8	78.6
-2	26.0	36.6	61.1	90.8	94.5	74.0	85.9	78.0	
-3	27.6	32.2	63.3	70.7	82.4	70.7	85.5	68.2	
-4	27.4	35.3	68.3	88.7	83.6	82.8	89.3	73.2	
Average	26.6	35.6	67.7	75.2	92.3	78.5	78.1	65.0	
45016B-1	19.7	23.7	33.5	36.2	32.4	40.8	49.1	61.9	
-2	19.5	22.0	33.3	37.6	31.6	38.5	55.7	70.8	
-3	18.6	21.4	29.7	33.4	30.1	34.6	53.0	77.0	
-4	18.3	20.6	32.3	33.3	31.3	41.2	61.2	84.4	
45016C-1	20.4	22.9	36.1	38.3	46.0	56.5	66.9	86.4	84.7
-2	19.5	23.8	32.9	34.5	46.2	57.8	75.1	83.9	81.5
-3	19.6	22.5	35.8	40.1	50.5	64.2	71.6	78.5	78.8
-4	18.5	22.7	35.2	36.5	49.4	62.5	73.0	81.4	94.2
Average	19.3	22.5	33.6	36.3	39.6	49.5	63.3	78.0	84.8
45018B-1	20.7	23.2	33.6	31.4	27.6	37.3	54.4	58.8	61.6
-2	20.4	22.9	31.1	31.4	23.2	37.3	50.4	52.5	65.9
-3	22.3	24.4	35.0	34.4	46.0	58.7	53.6	58.7	
-4	20.8	25.5	36.4	33.9	43.4	57.0	54.8	63.1	67.1
Average	21.0	24.0	34.0	32.8	35.2	47.6	53.3	58.3	64.9

TABLE V

SPECTRAL INTENSITY DATA

ANNEALING TEMPERATURE: 500°C

INTEGRATED RED-TO-INFRARED RATIO

Diode	ANNEALING TIME (HOURS)								
	0	2	4	8	12	16	24	32	50
44345A-1	27.6	89.2	139.4	207.8	129.0	110.8			114.4
-2	30.8		174.1	164.4	197.8	86.5		125.9	121.1
-3	32.5	93.1	162.5	148.3	141.0	98.3		124.5	154.4
-4	30.3	89.3	134.6	193.8	191.8	113.9		163.1	121.1
-5	30.1	55.4	168.8	148.8	148.1	140.9		145.1	161.2
Average	30.3	81.8	155.9	172.6	161.5	110.1		139.7	134.4
45016A-1	20.6	31.4	45.0		68.1	74.6	101.0	78.5	97.9
-2	20.3	28.7	47.5	59.1	62.1	66.7	79.8	59.1	92.3
-3	19.7	34.2	45.1	63.4	66.9	67.1	90.2	80.9	71.5
-4	19.8	34.4	43.0	48.2	66.5		83.8	83.7	81.4
-5	19.7	34.0	45.3	51.0	65.9	60.9	86.9	64.5	88.2
Average	20.0	32.5	45.2	55.4	65.9	67.3	88.3	73.3	84.3
45018A-1	8.8	31.2	47.9	52.0	68.1	54.7	84.3	94.0	90.7
-2	9.3	35.5	50.0	58.8	75.4	60.9	93.1	101.8	103.8
-3	16.3	34.4	50.6	54.8	87.3	77.2	108.1	98.7	96.7
-4	9.4	36.2	49.1	65.2	84.0	71.2	88.0	94.8	
-5	19.0	38.1	44.9	65.6	90.5	68.2	83.7	90.3	
Average	12.6	35.1	48.6	59.3	81.1	66.4	91.4	95.9	97.1

ENERGY LEVEL DIAGRAM OF Zn,O IN GaP
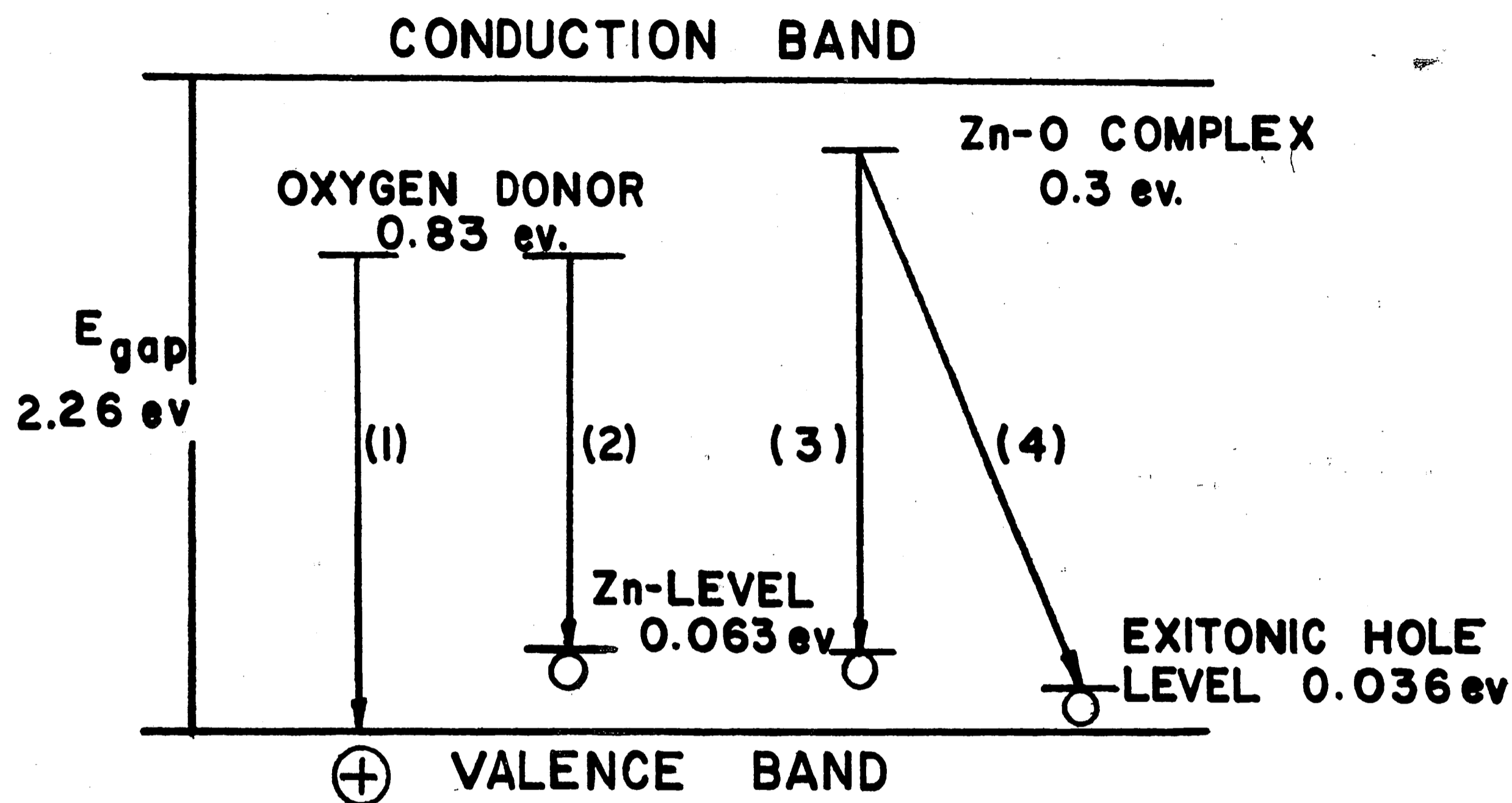
(1) BOUND-TO-FREE RECOMBINATION

(2) DONOR-ACCEPTOR PAIR RECOMBINATION

(3) PAIR RECOMBINATION BETWEEN ELECTRON TRAPPED AT Zn-O AND HOLE AT ZINC

(4) EXITONIC RECOMBINATION

FIGURE I

FIGURE 2

$H_2 + N_2$

$Ga + GaP + Zn + Ga_2O_3$

GaP SUBSTRATE
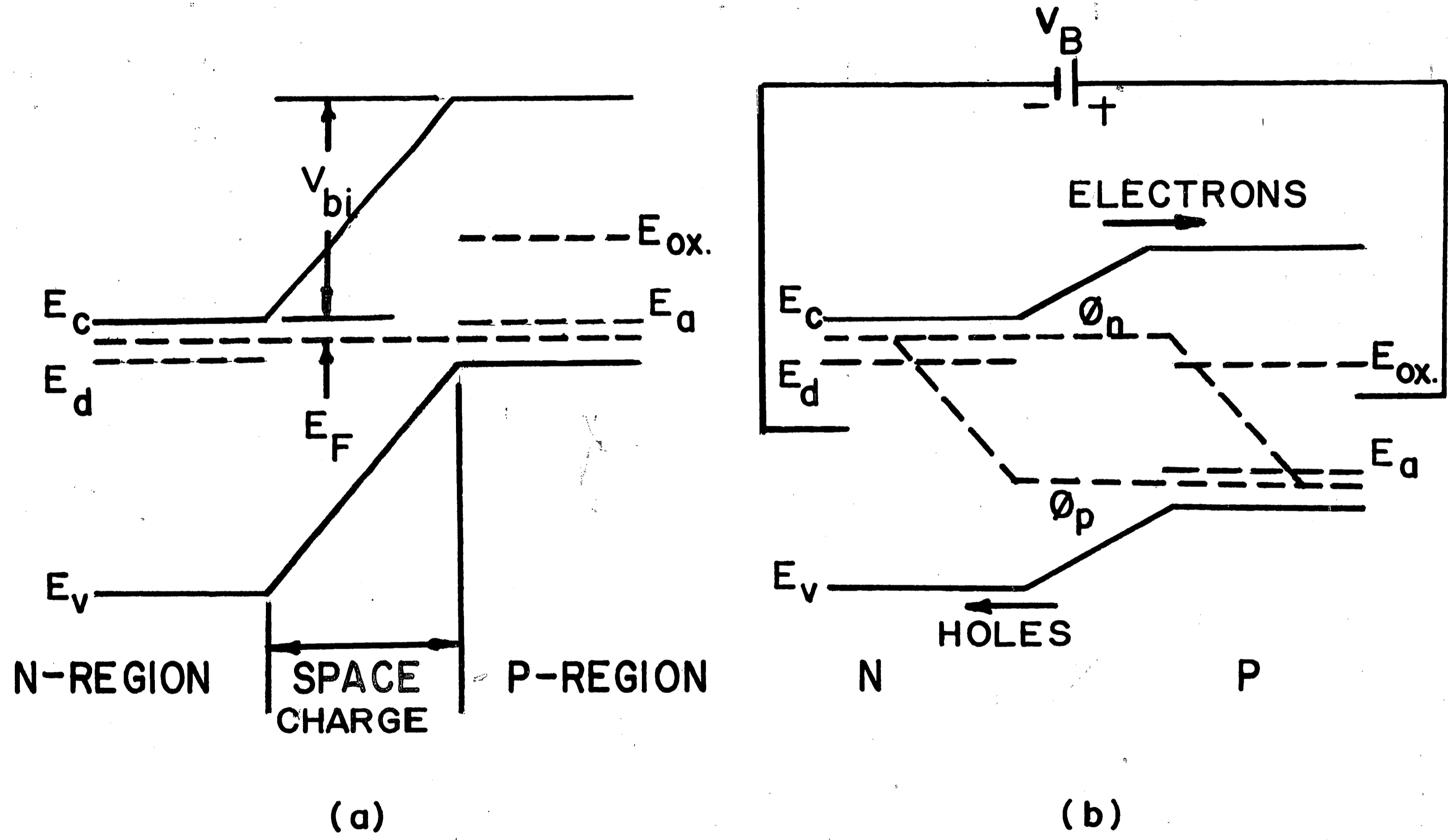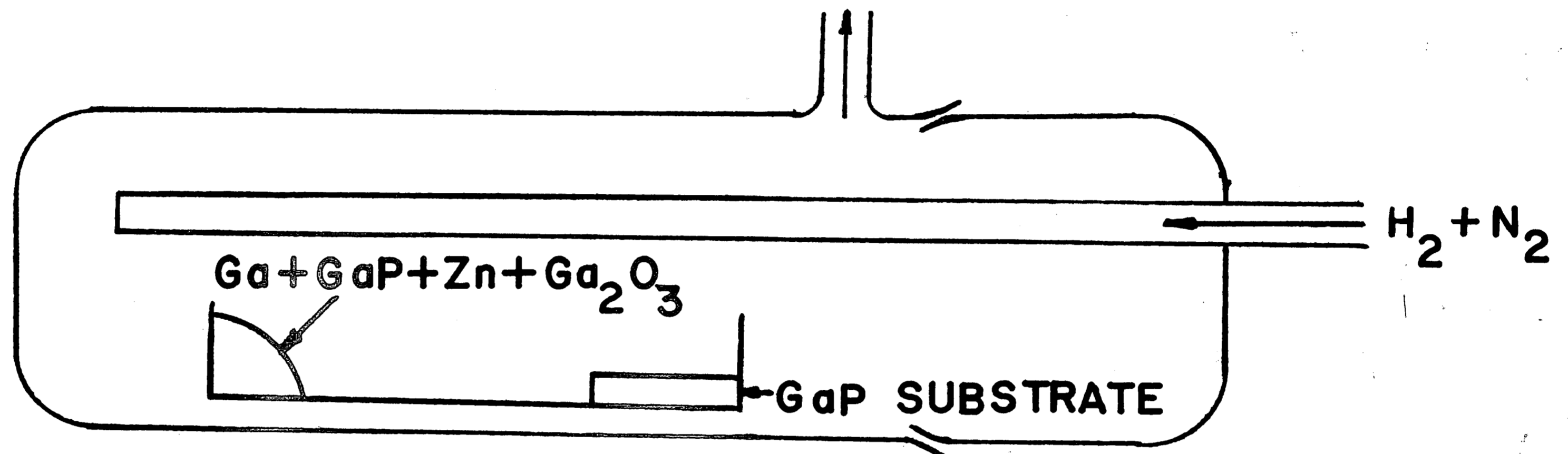
GaP LIQUID-PHASE EPITAXY SYSTEM

LPE LAYER

BEFORE TIPPING   AFTER TIPPING

FIGURE 3

2 % Zn-DOPED Au ALLOY CONTACT

EVAPORATED Au SCHOTTKY DIODES

(Zn,O) P-EPI

Te-DOPED N-EPI

Se-DOPED N-SUBSTRATE

2 % Sn-DOPED Au ALLOY CONTACT

θ
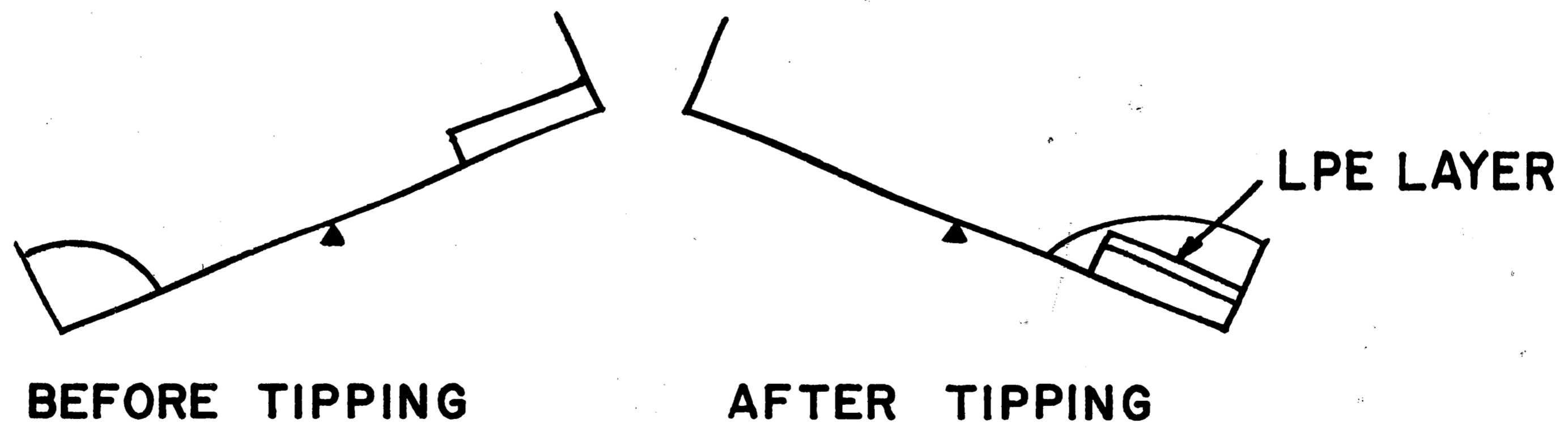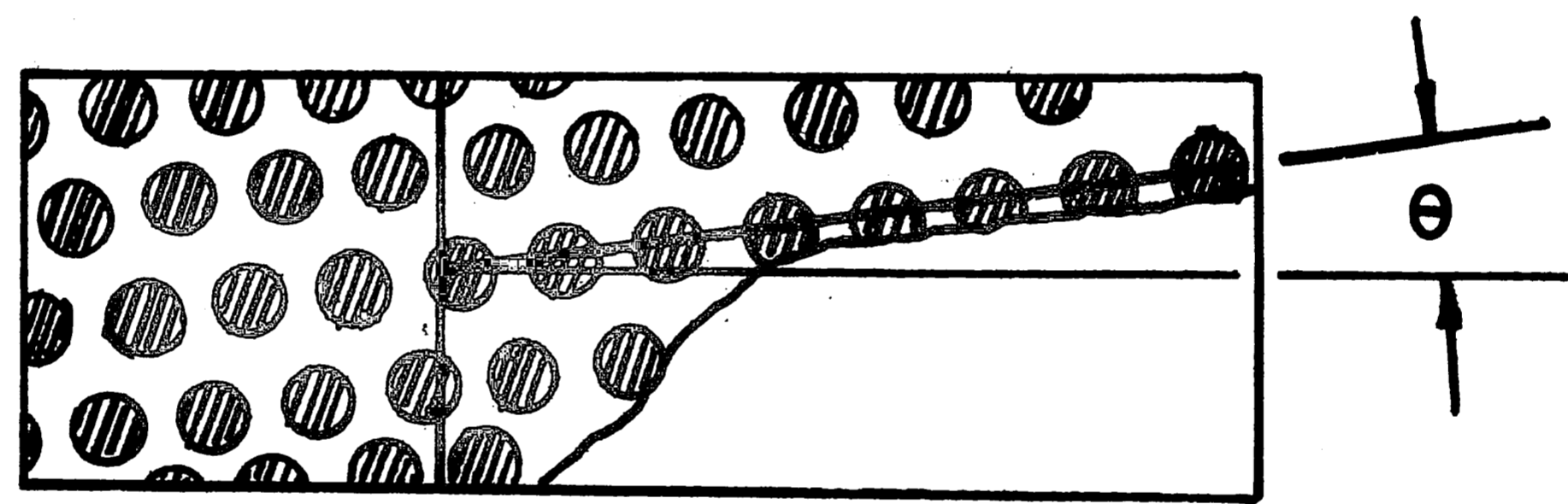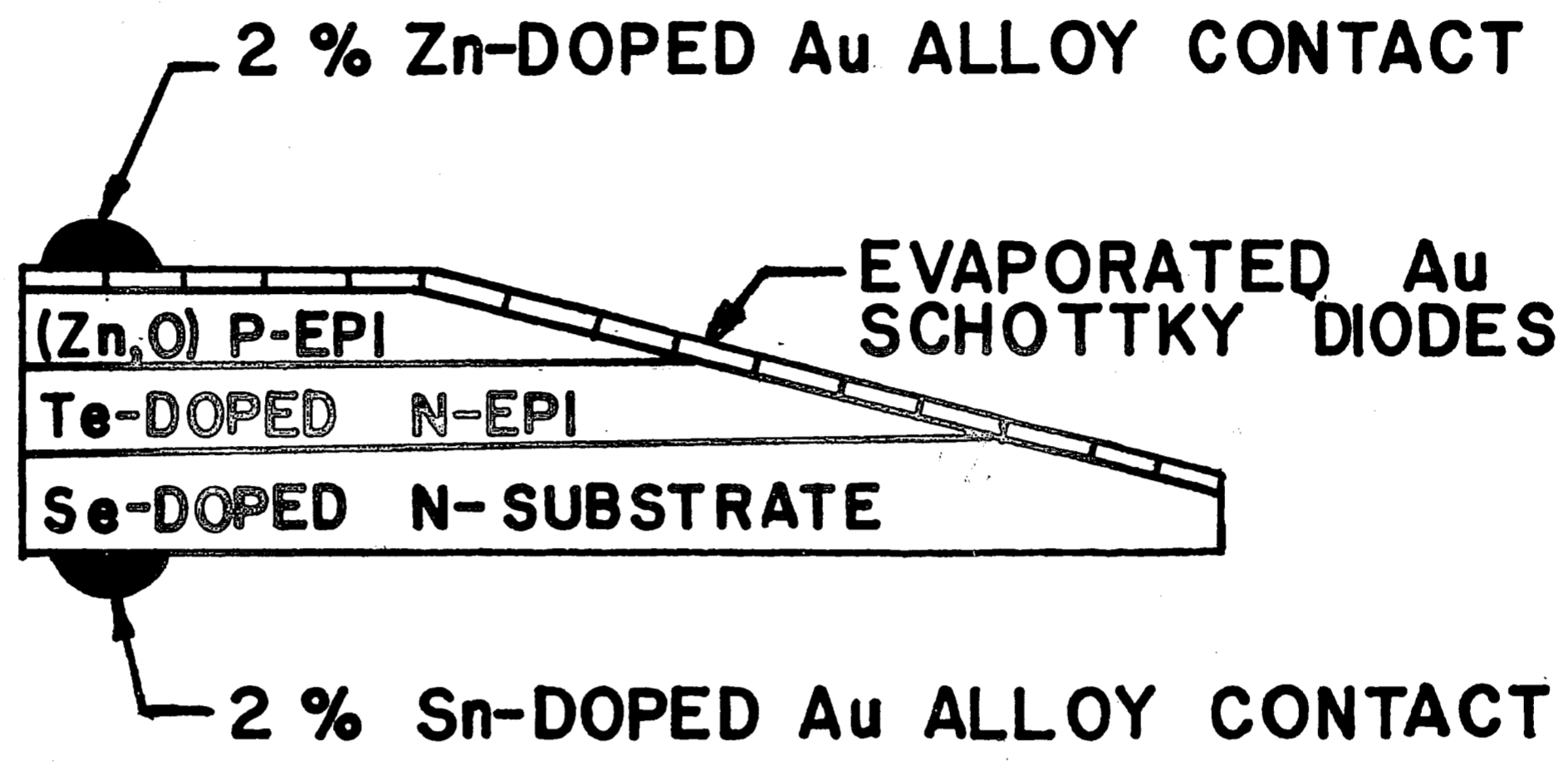
FIGURE 4

FIGURE 5

FIGURE 6

$N_D - N_A (10^{18} CM^{-3})$
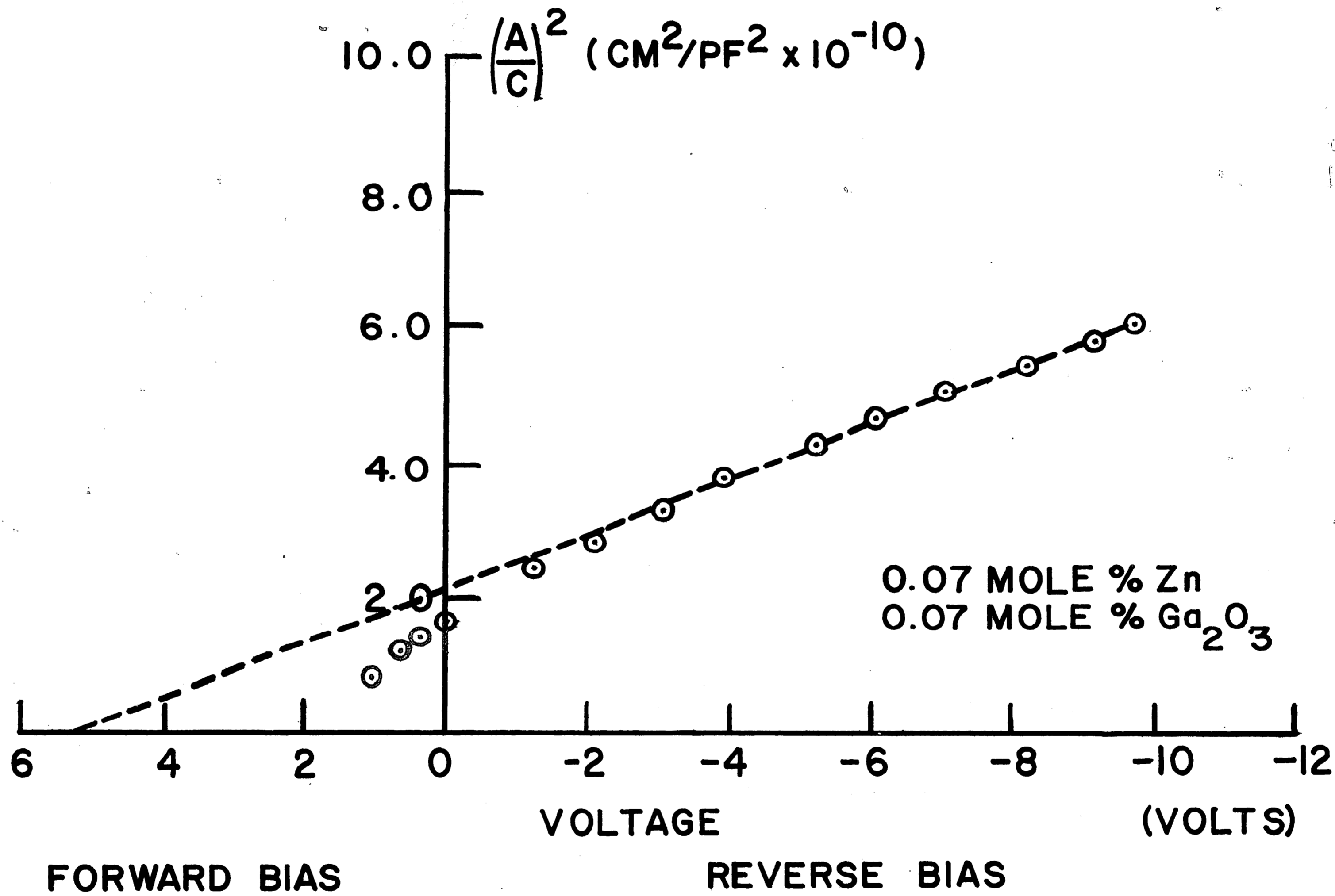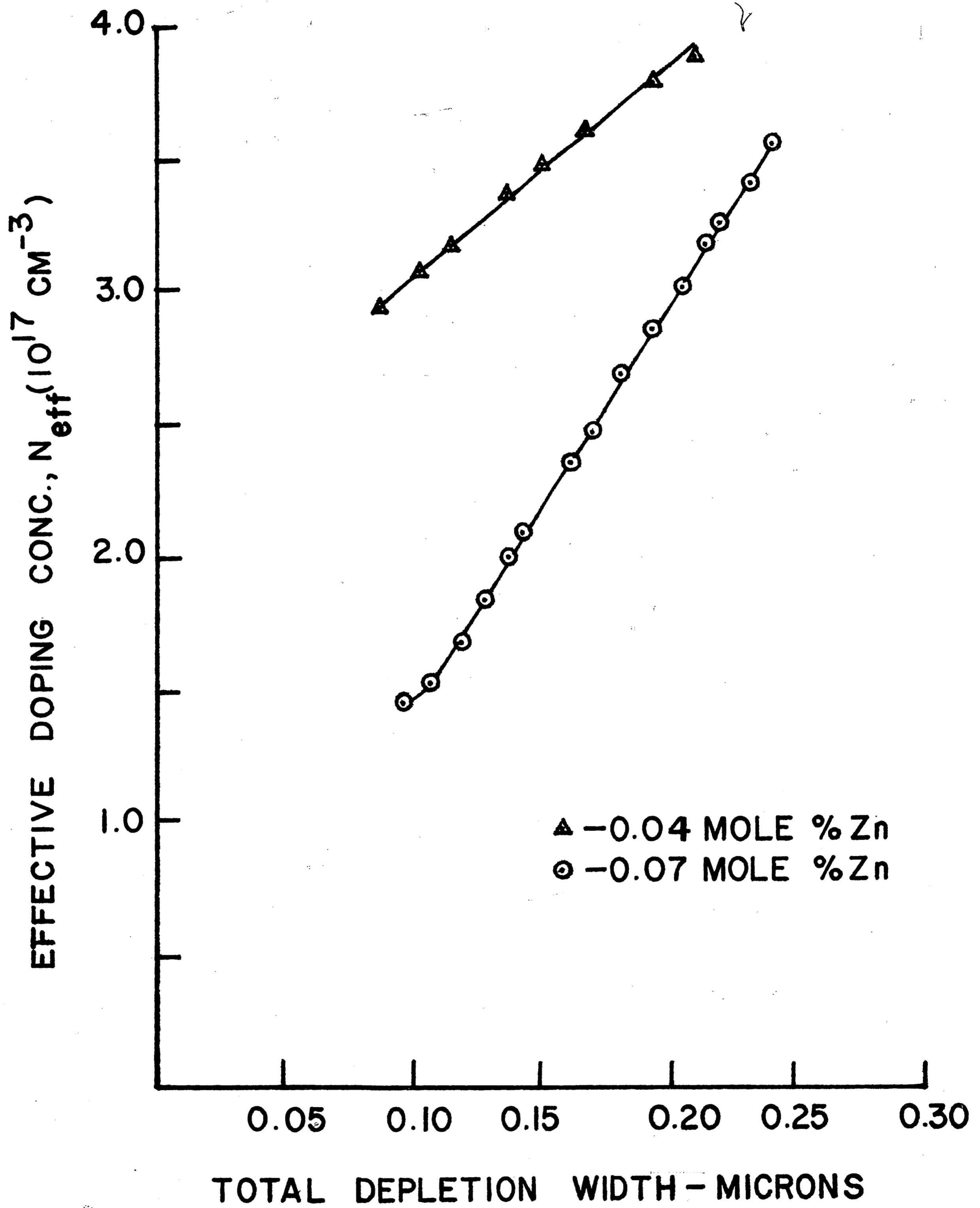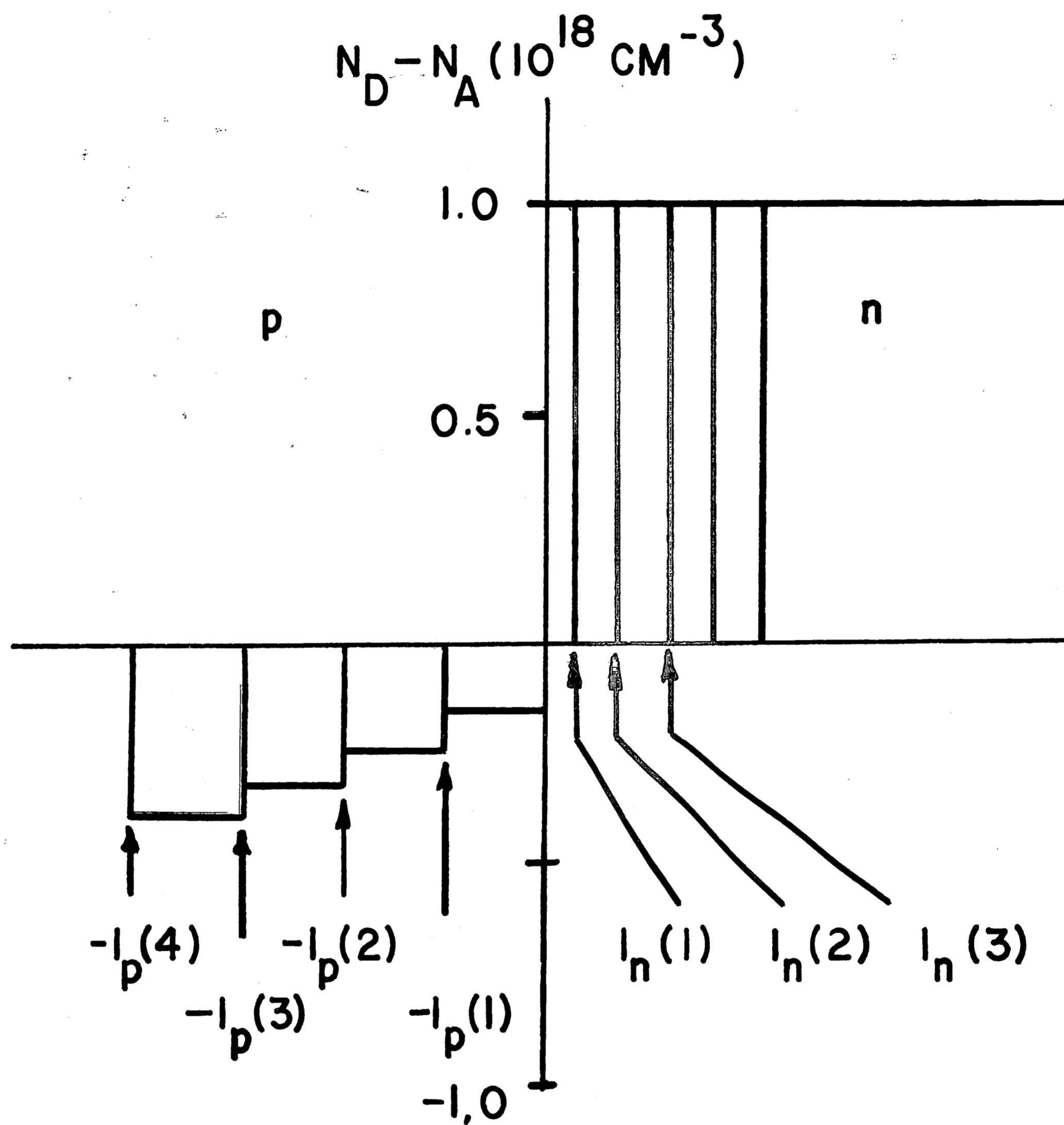
$$(1) \quad N_A(i) = \frac{N_D \cdot N_{eff}(i)}{N_D - N_{eff}(i)}$$

$$(2) \quad I_p(i) = I_p(i-1) + \frac{N_D \left[I_t(i) - I_t(i-1) \right]}{N_A(i-1) + N_D}$$

FIGURE 7

SOLAR PANEL

ABSORPTION FILTER

ALUMINIZED SURFACE

SAMPLE

I

CURRENT SUPPLY
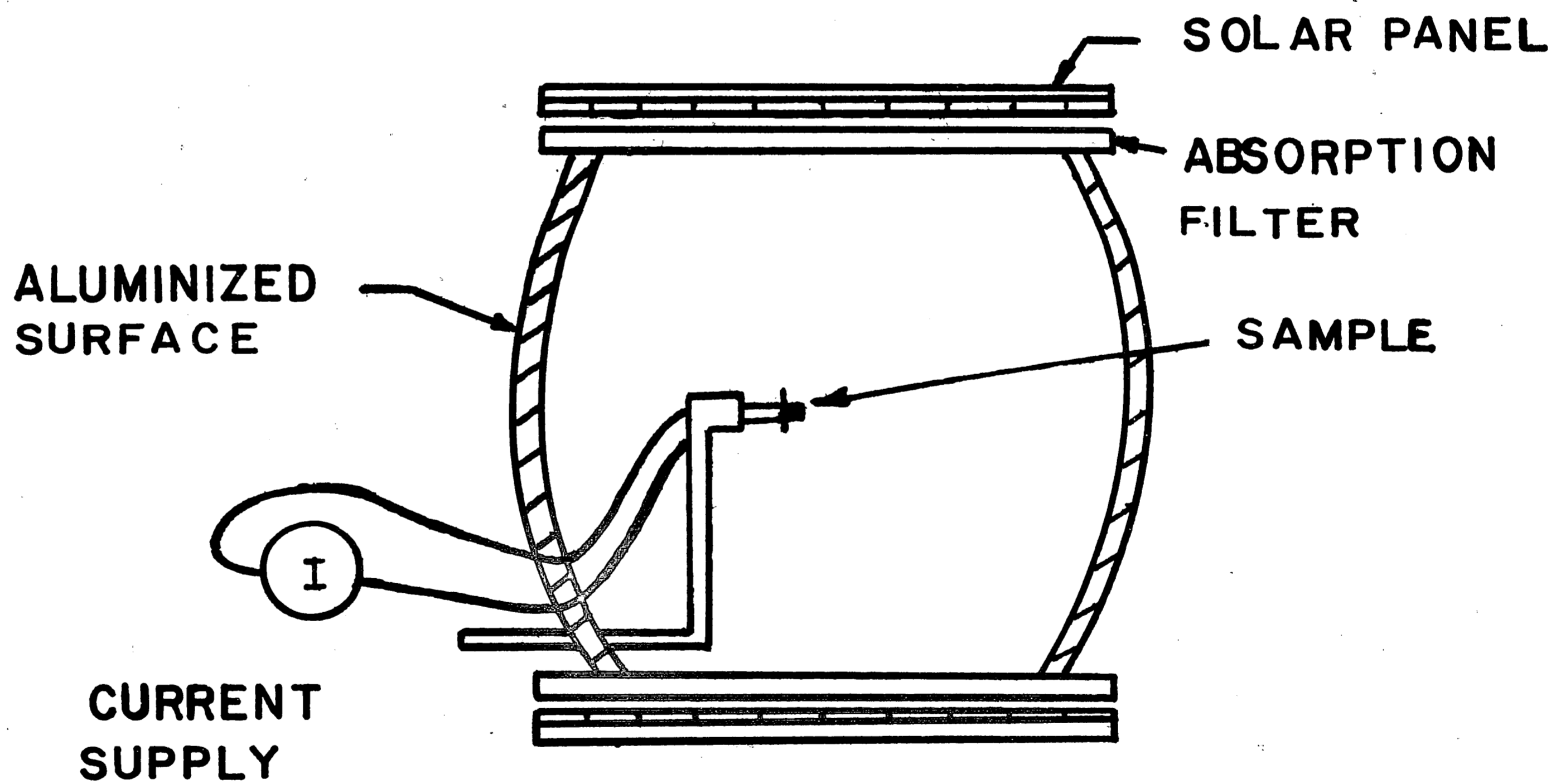
ELECTROLUMINESCENT EFFICIENCY TEST SET

FIGURE 8

FIGURE 9

P - REGION

$N_A - N_D$ $(10^{18}$ CM$^{-3})$

WAFER: 450-16

0.04 MOLE % Zn

0.07 MOLE % Ga$_2$O$_3$

N - REGION

FIGURE 10

FIGURE II

P — REGION

$N_A - N_D$ $(10^{18} CM^{-3})$

WAFER: 450-18
0.04 MOLE % Zn
0.07 MOLE % Ga_2O_3

N-REGION

(μM)
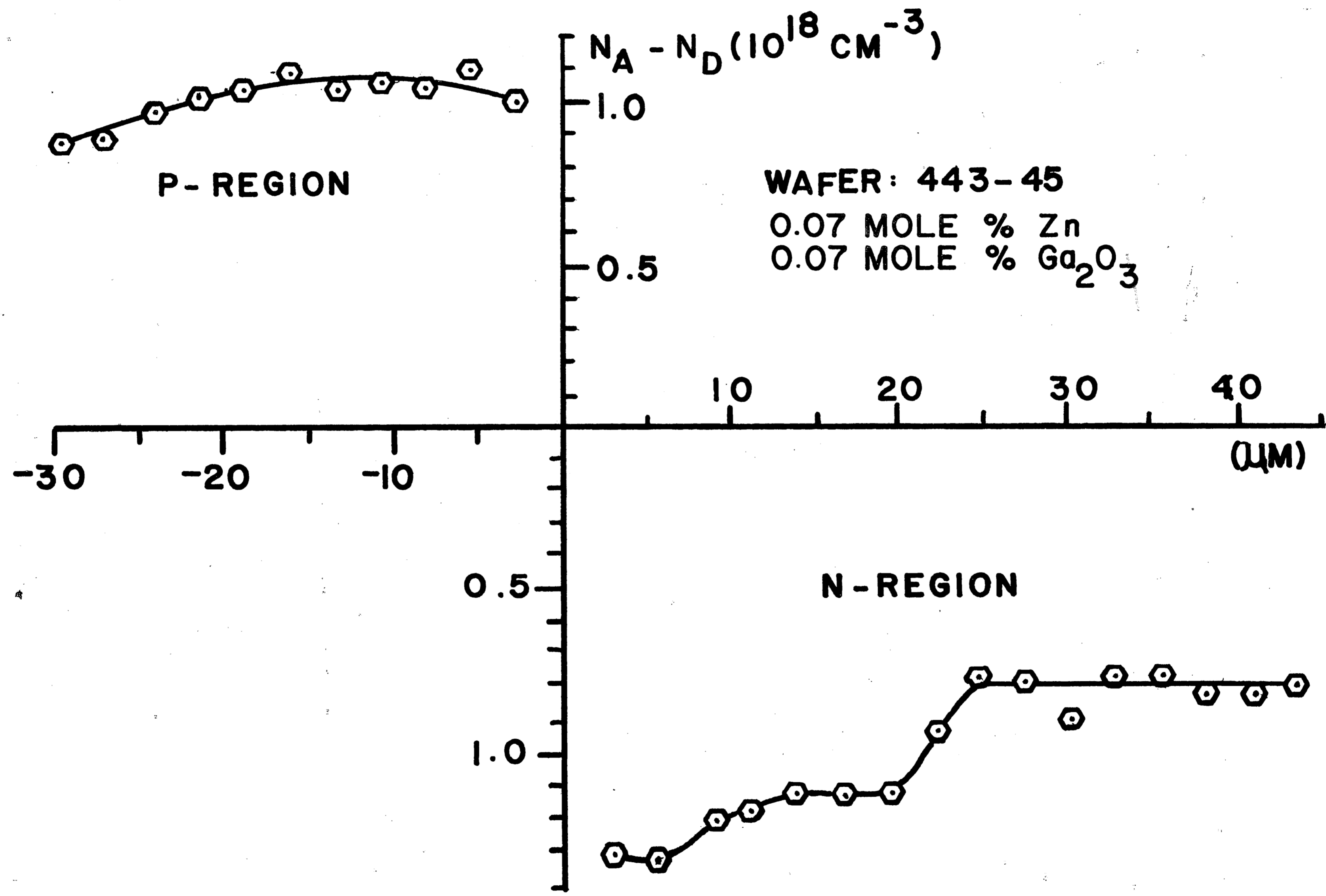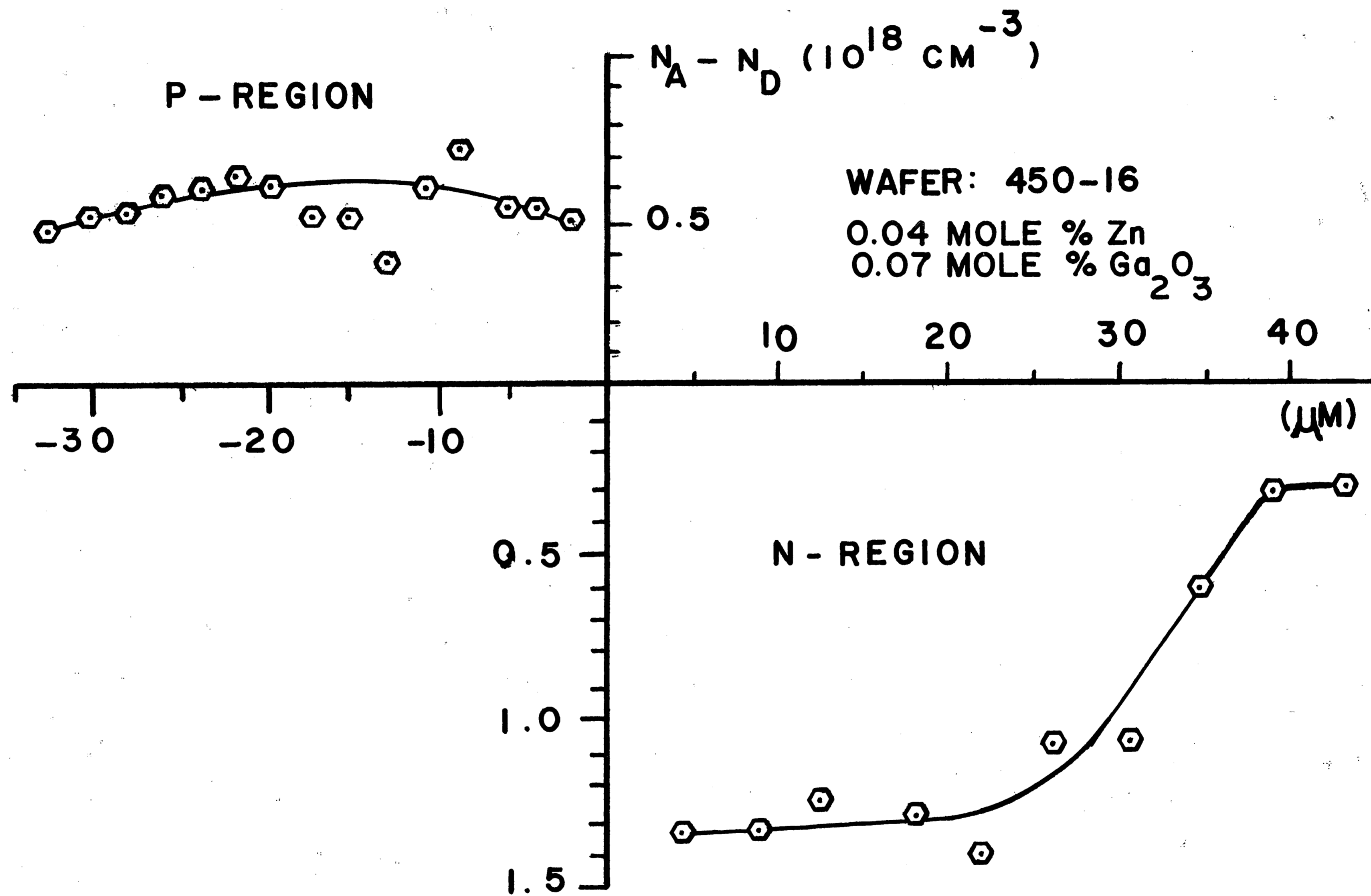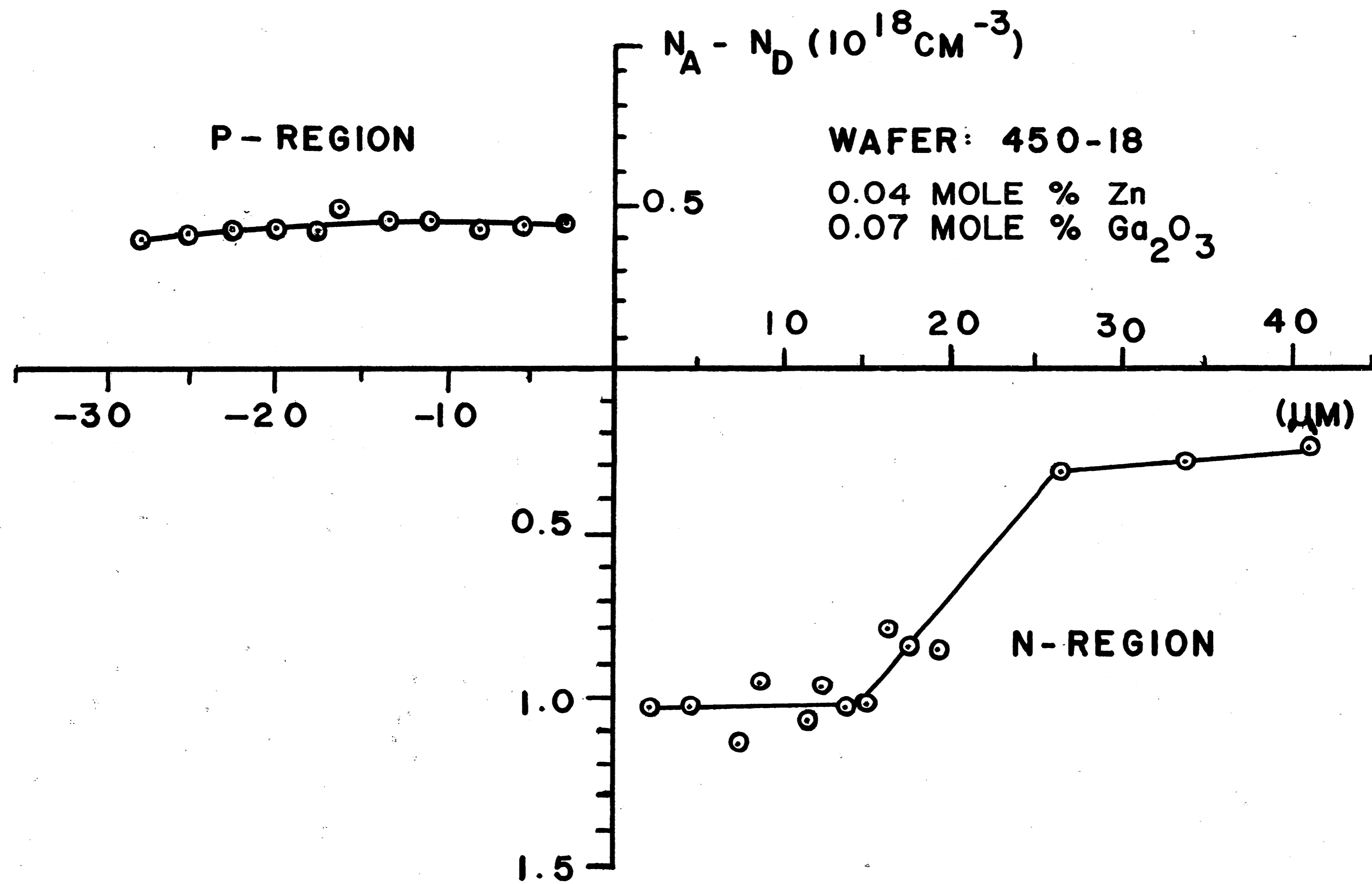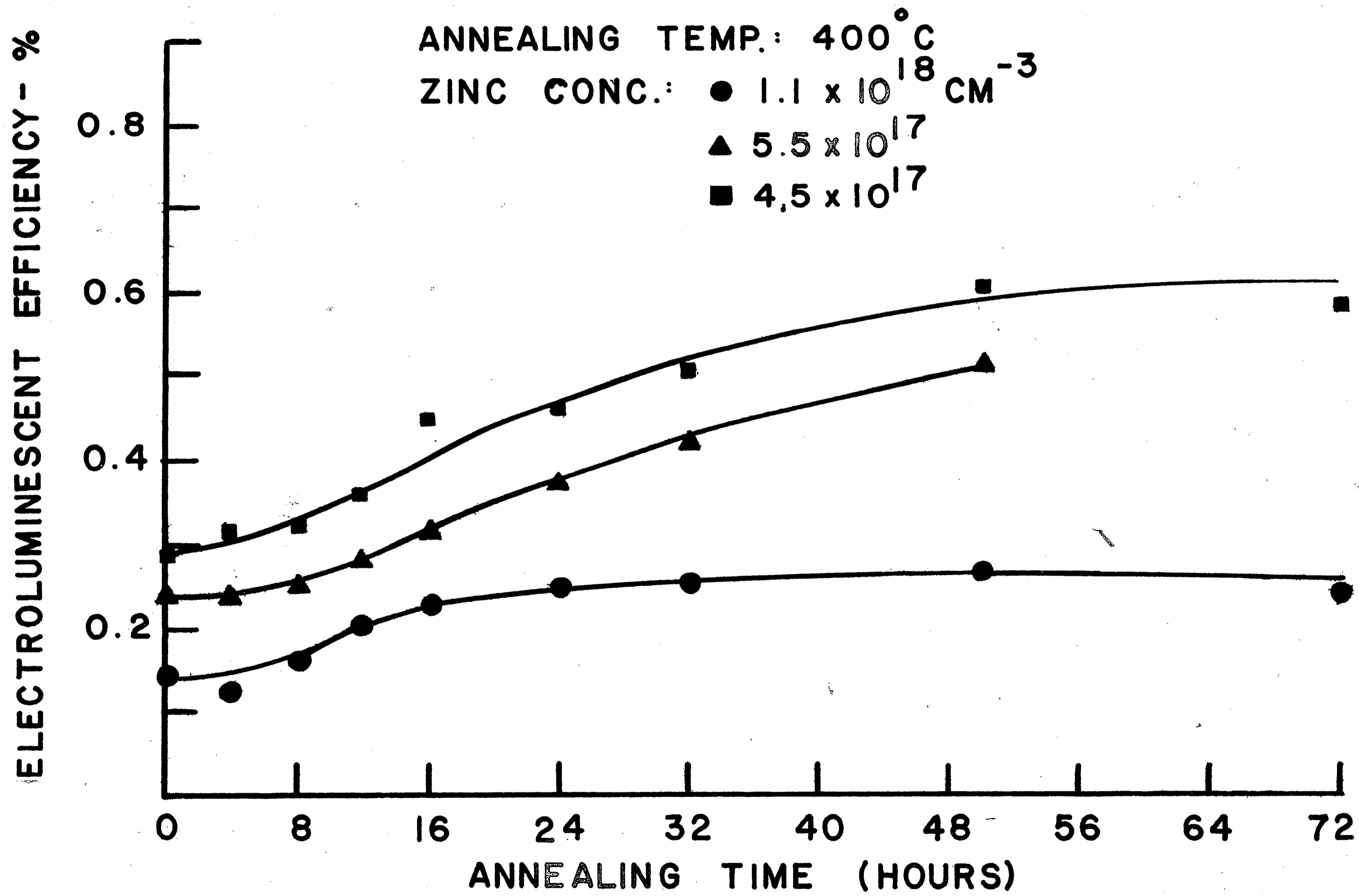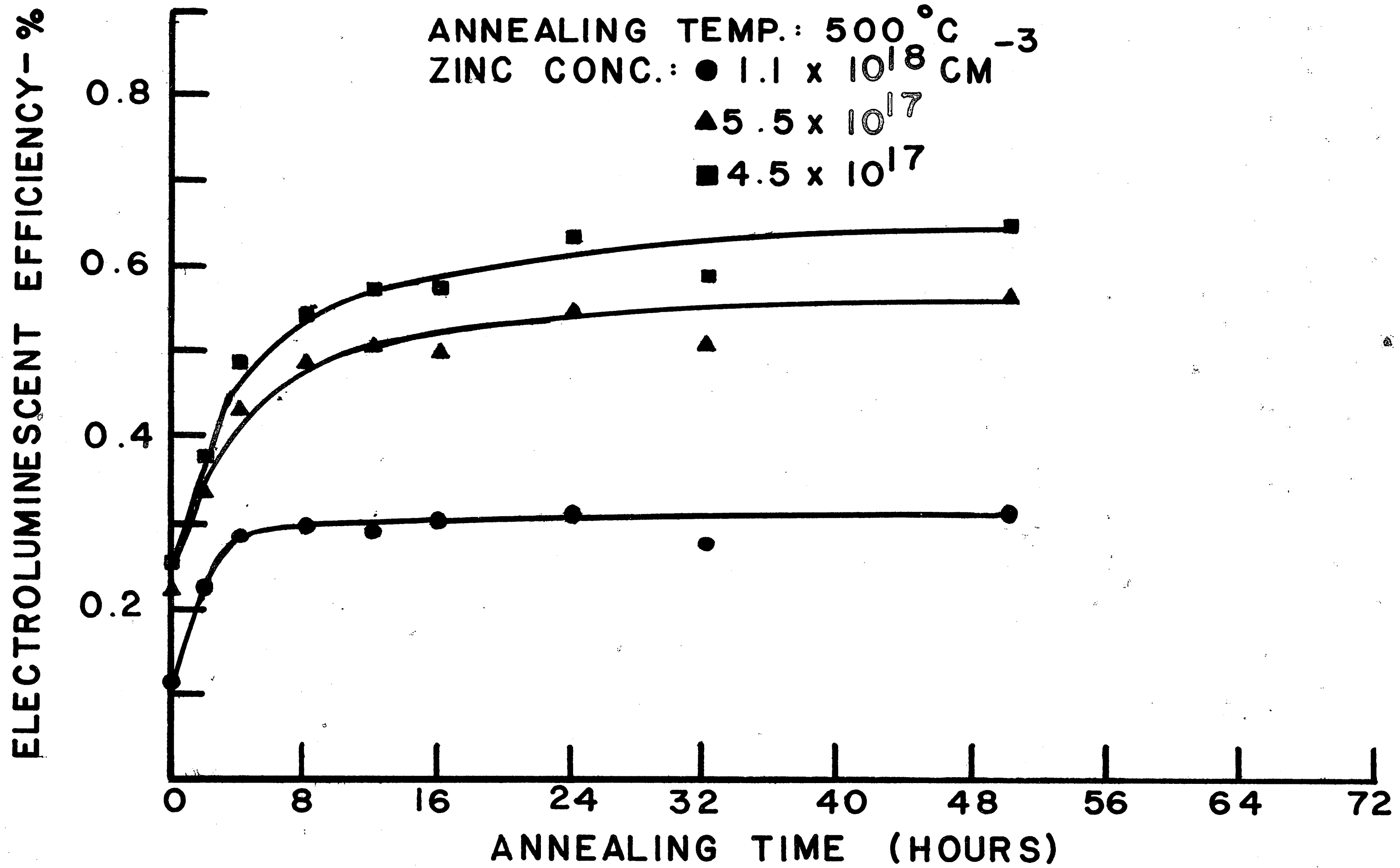
FIGURE 12

FIGURE 13

FIGURE 14

WAVELENGTH (ANGSTROMS)
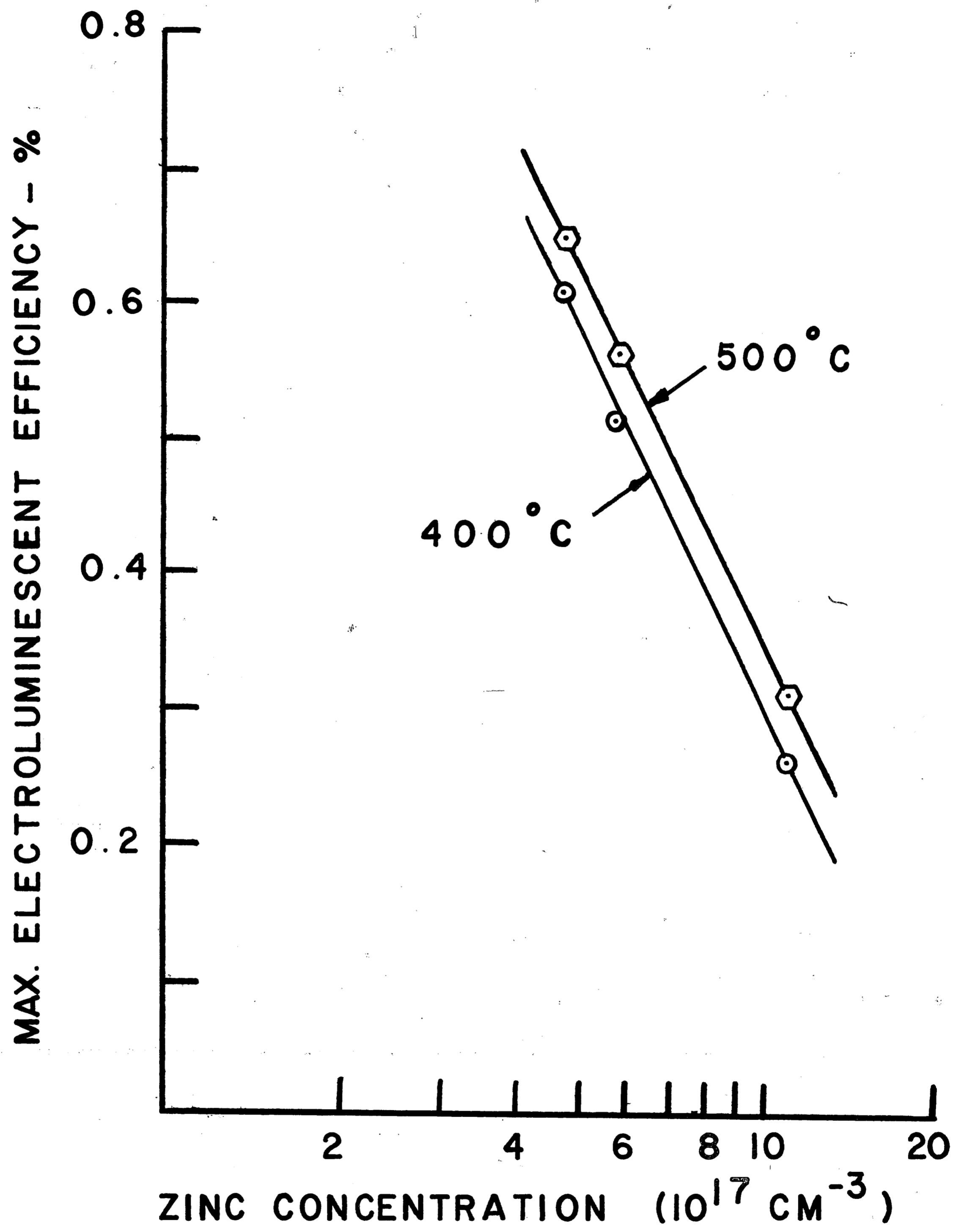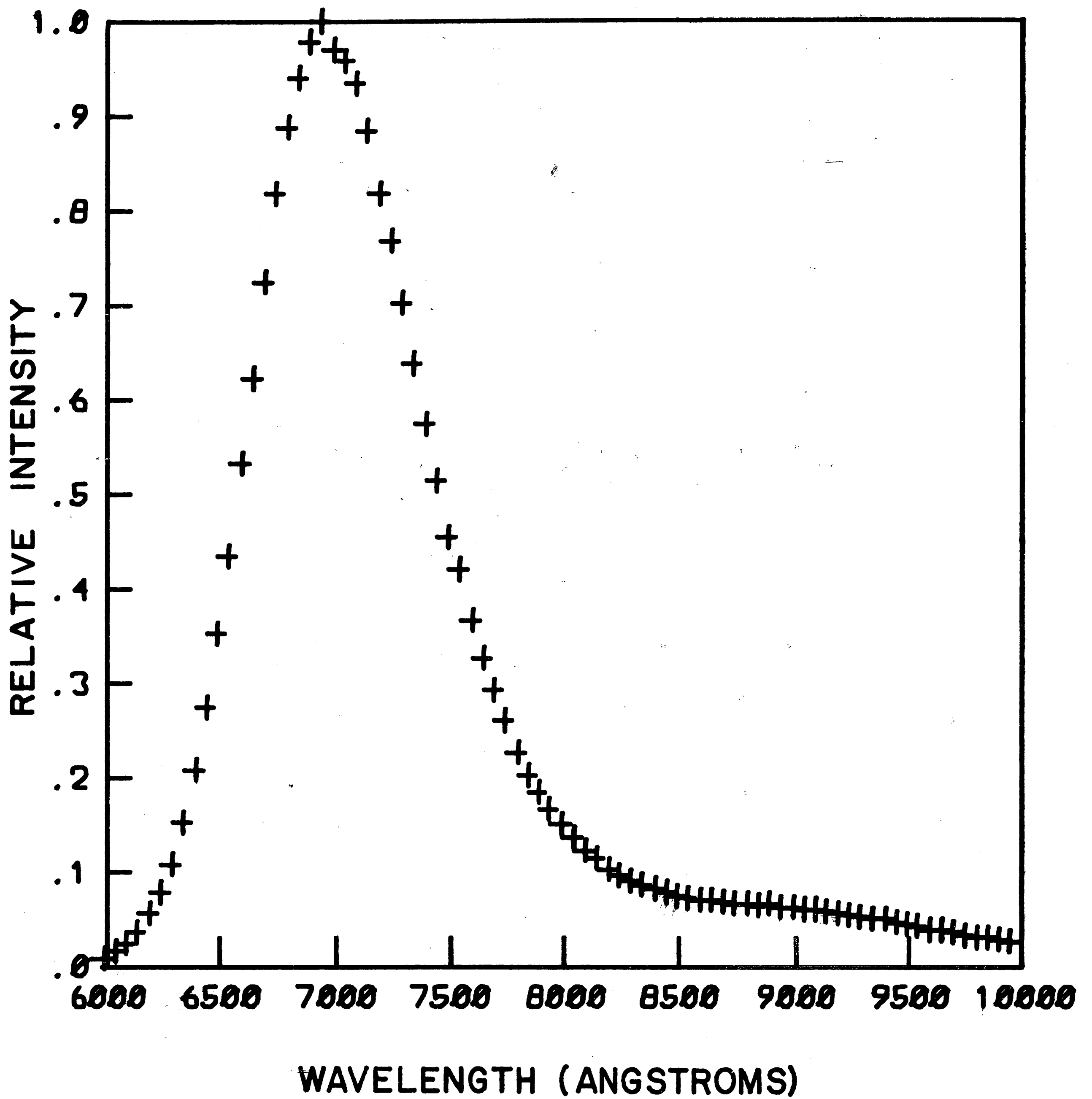
DIODE: 443-45A3 (UNANNEALED)
DIODE CURRENT: 10 MA.
TEMPERATURE: 500°C

FIGURE 15

-75-
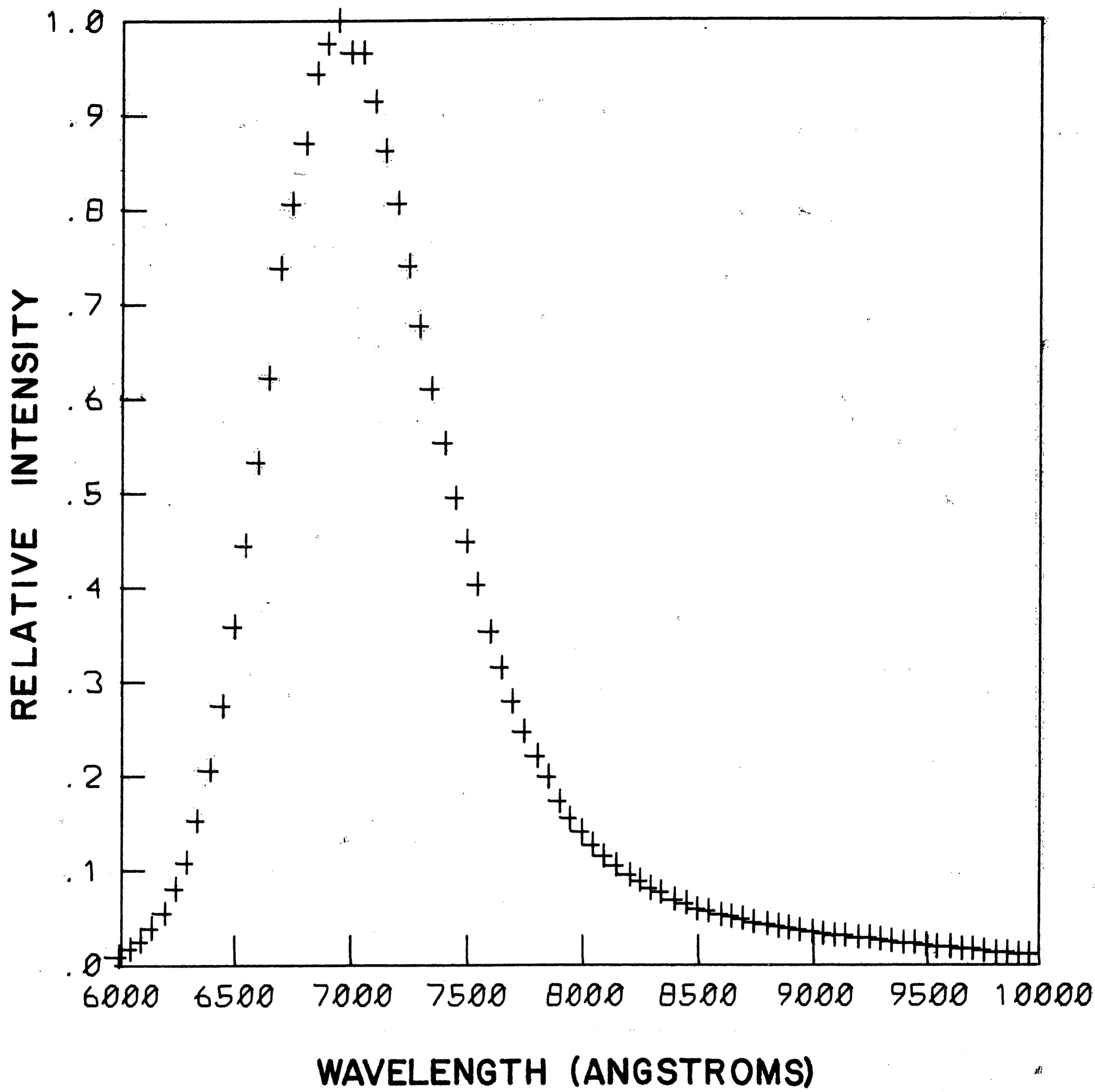
DIODE: 443-45A3 (ANNEALED)
DIODE CURRENT: 10 MA.
TEMPERATURE: 500 °C

FIGURE 16

WAVELENGTH (ANGSTROMS)
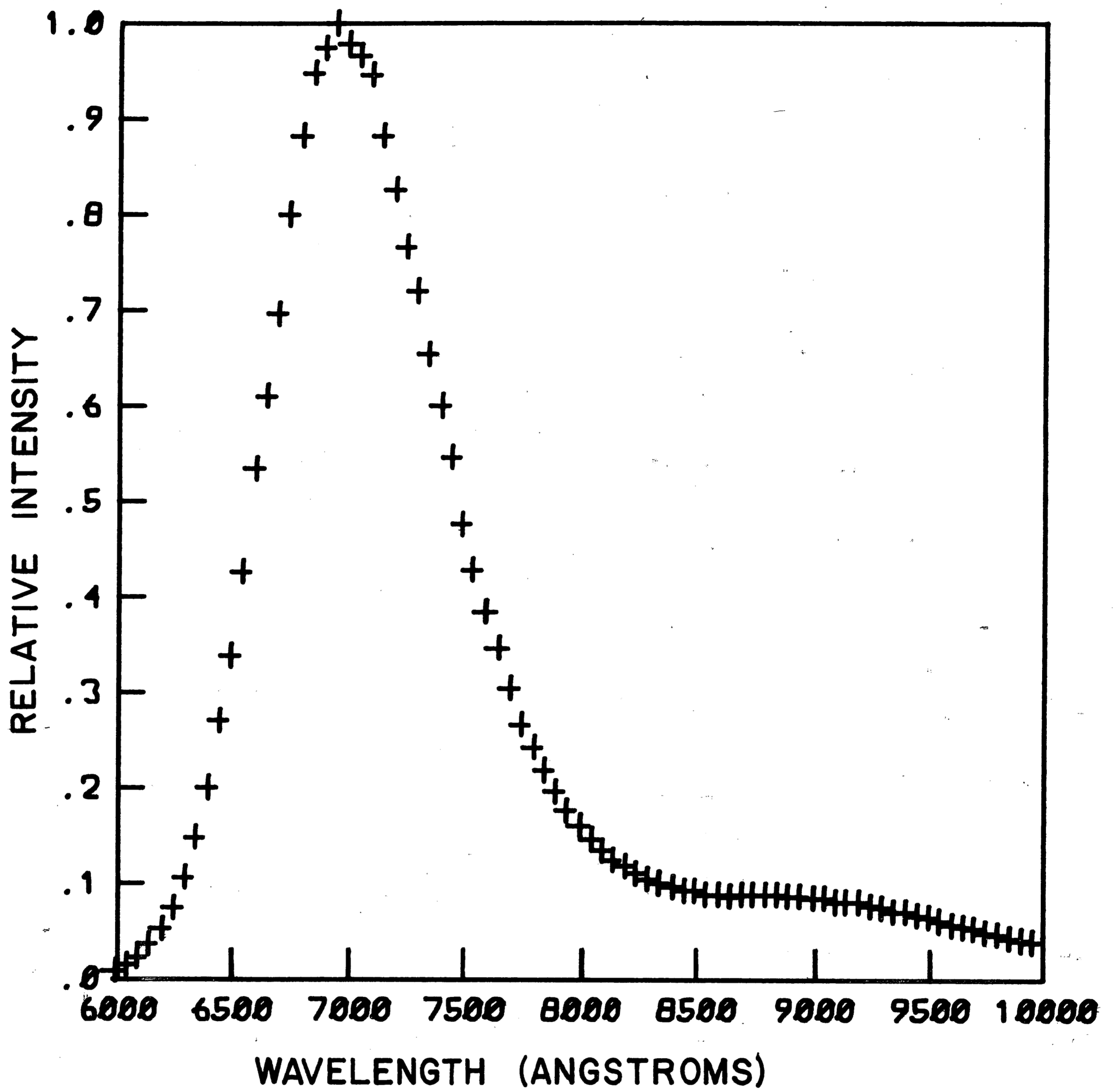
DIODE: 450-16A2 (UNANNEALED)
DIODE CURRENT: 10 MA.
TEMPERATURE: 500 °C

FIGURE 17
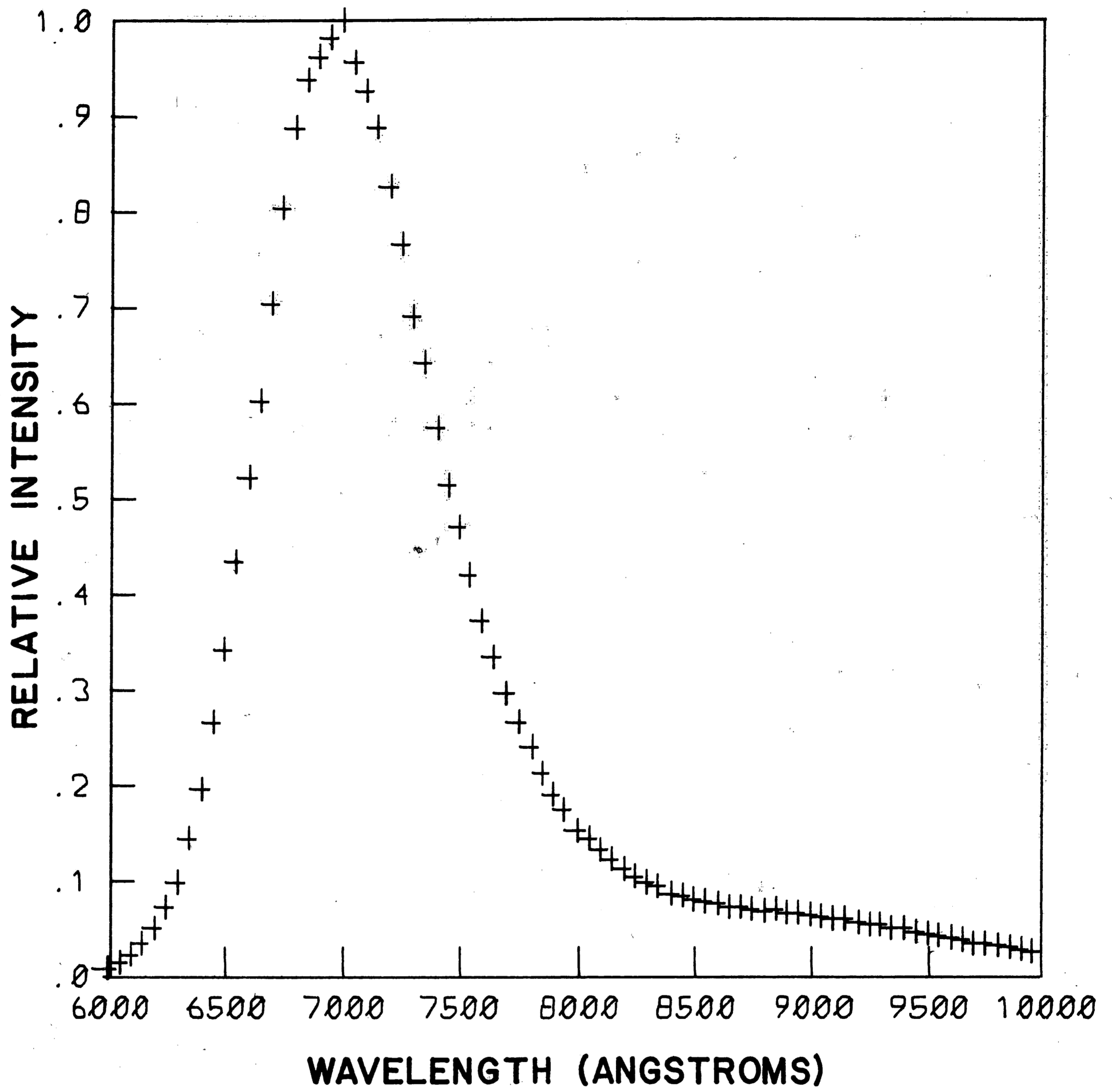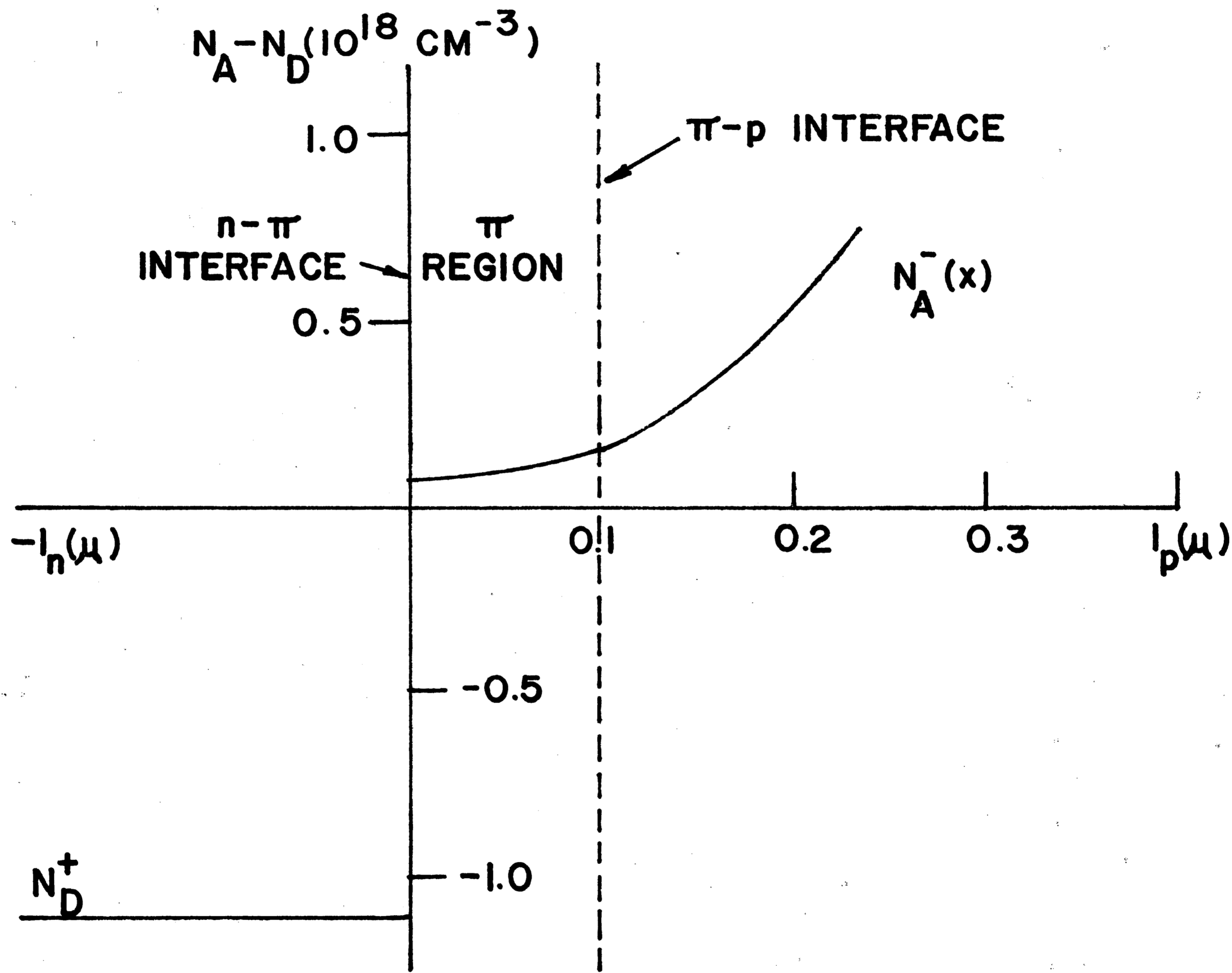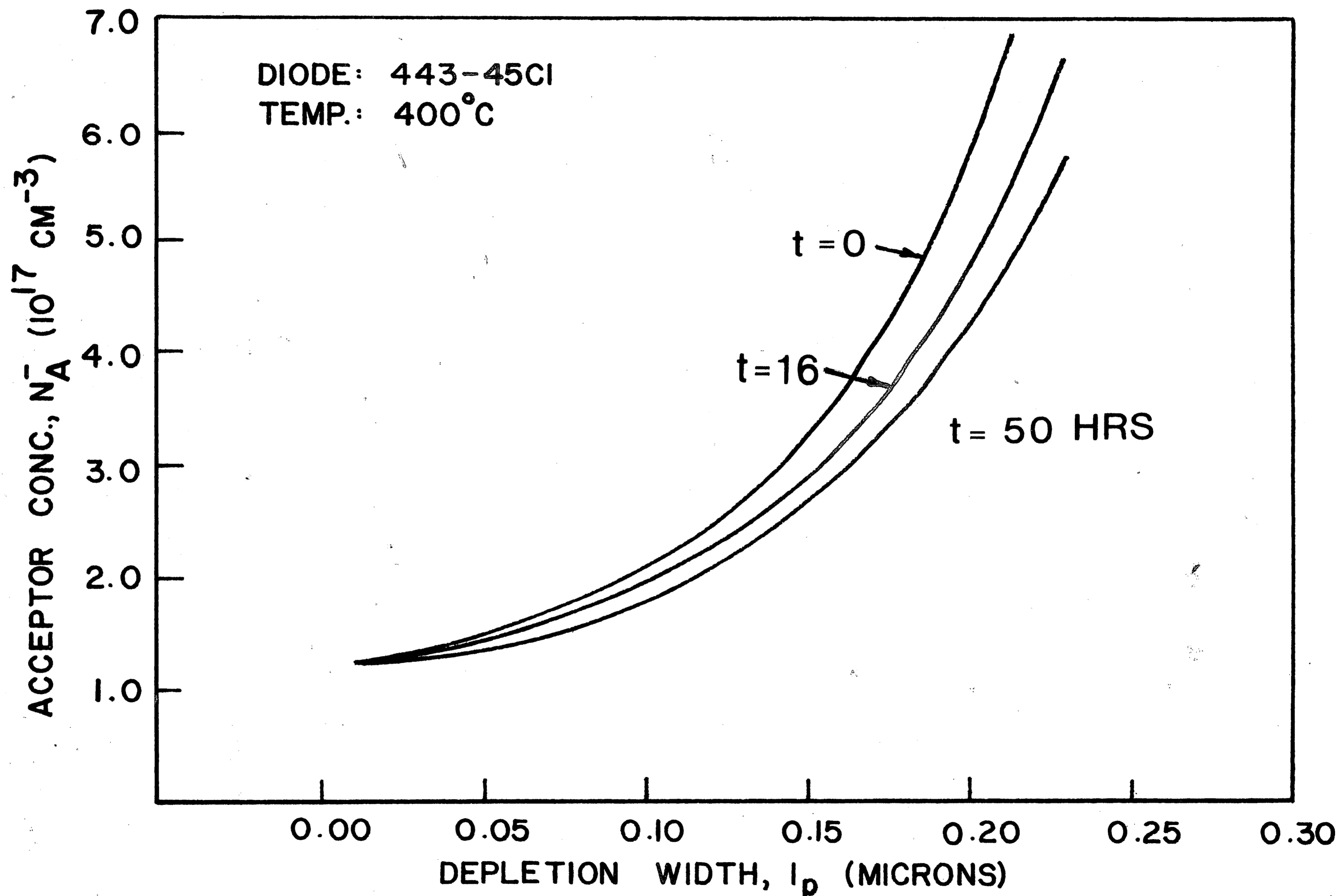
DIODE : 450-16A2 (ANNEALED)
DIODE CURRENT : 10 MA.
TEMPERATURE : 500°C

FIGURE 18
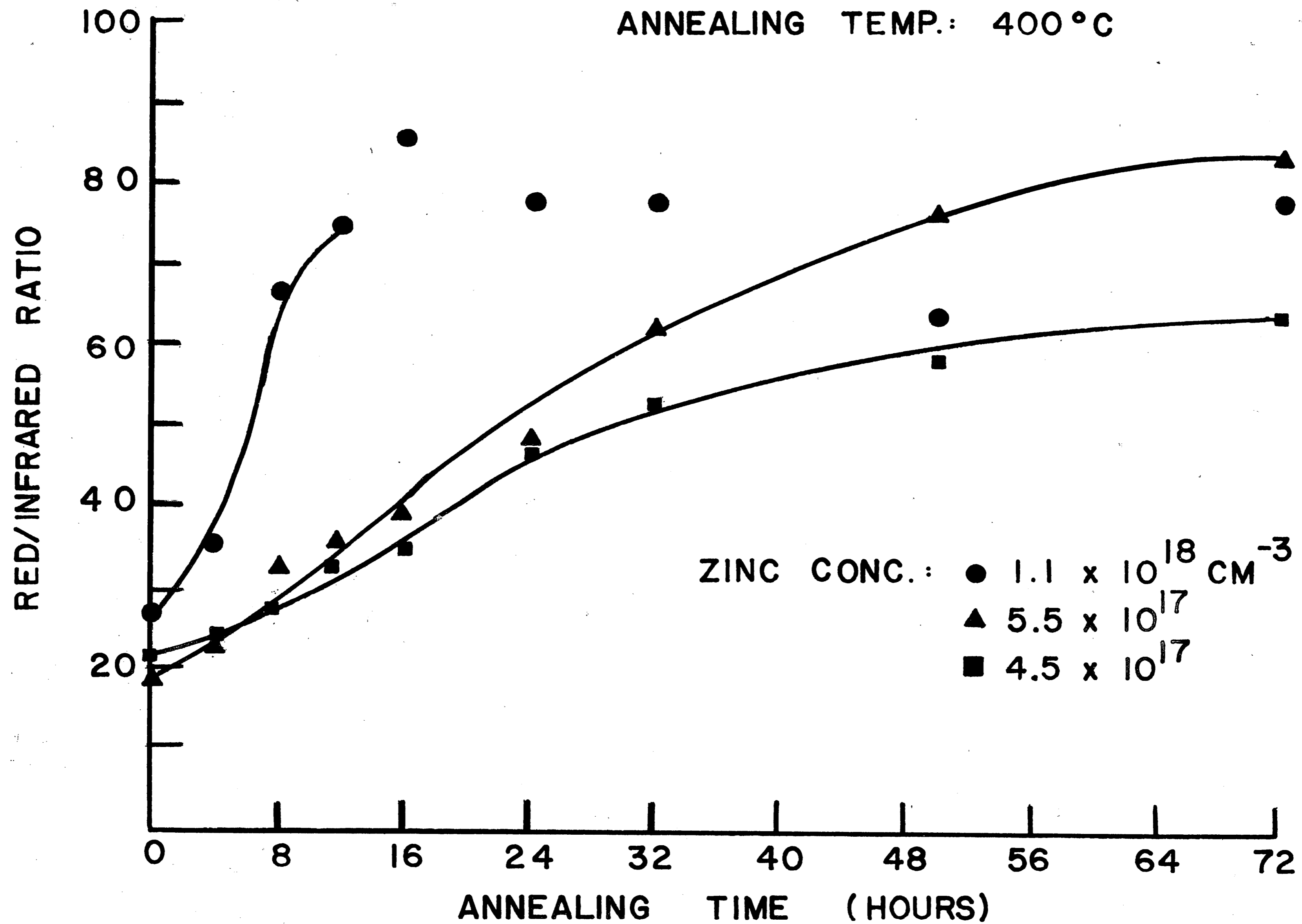
FIGURE 19

FIGURE 20

FIGURE 21

FIGURE 22

FIGURE 23

EFFECTIVE DOPING CONC., N_{eff} (10^{17} CM^{-3})

DIODE: 4 43-45 Al
TEMP.: 500°C

t = 0

t = 12

t = 24 HRS

DEPLETION WIDTH, l_t (MICRONS)
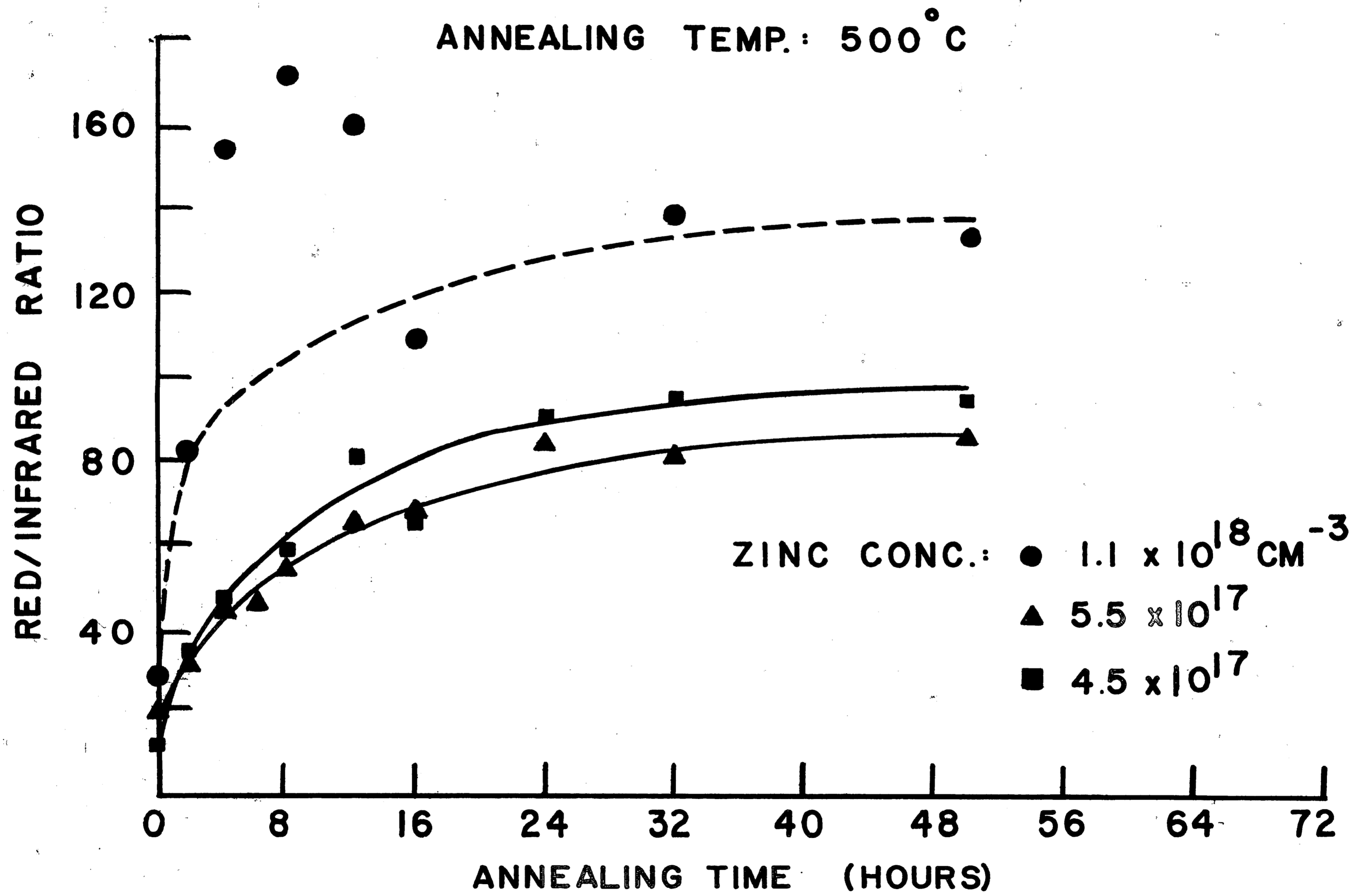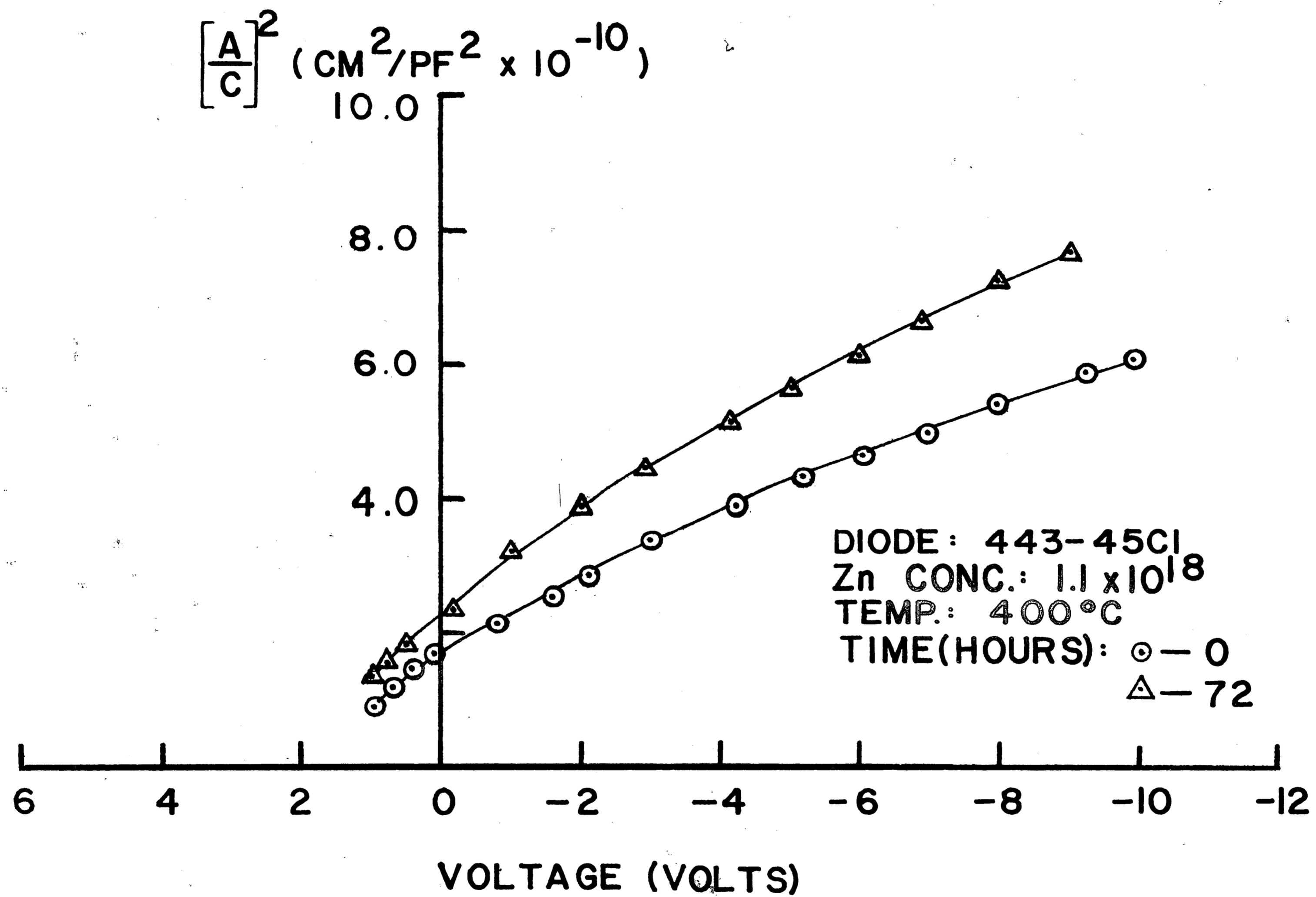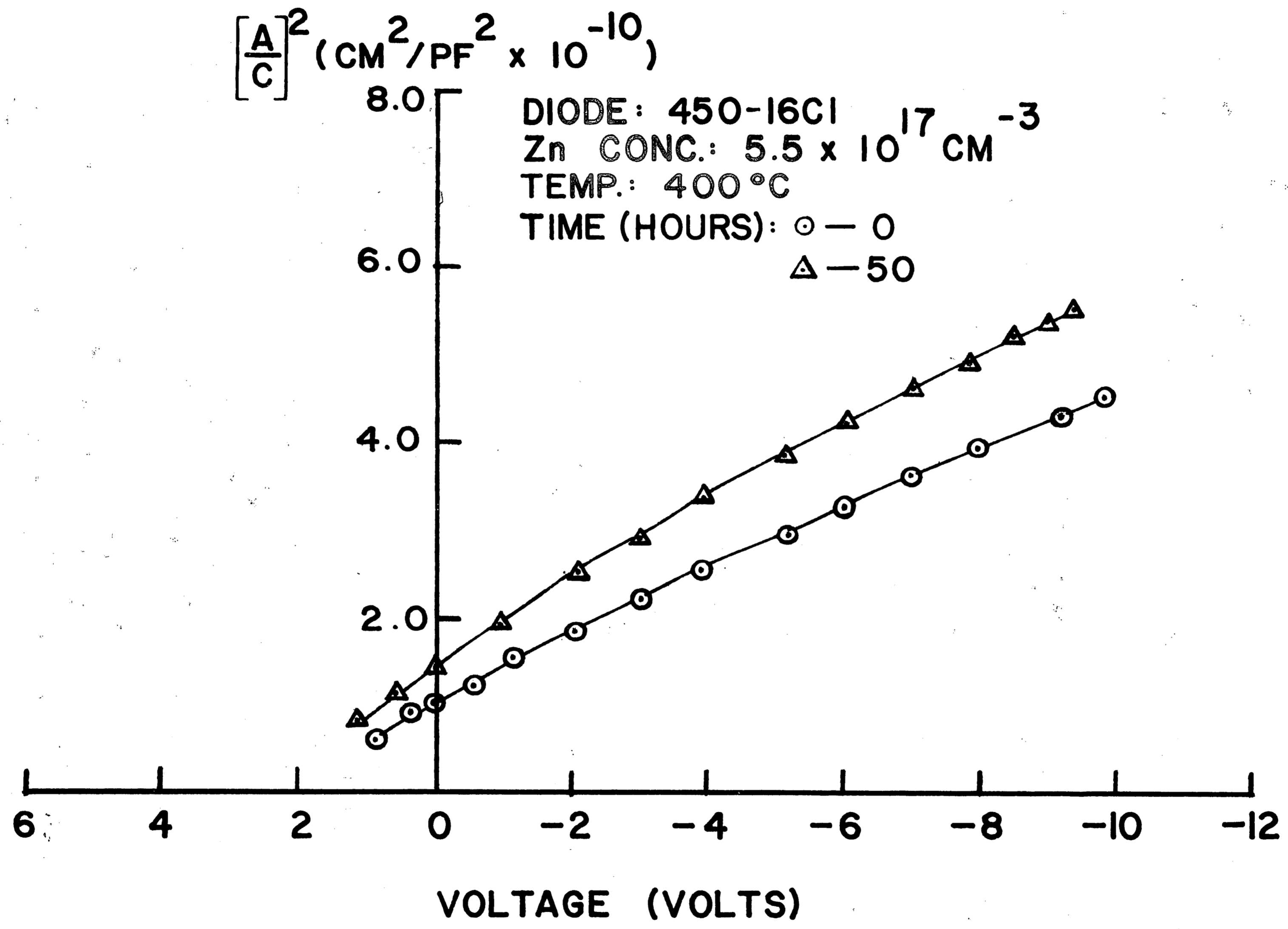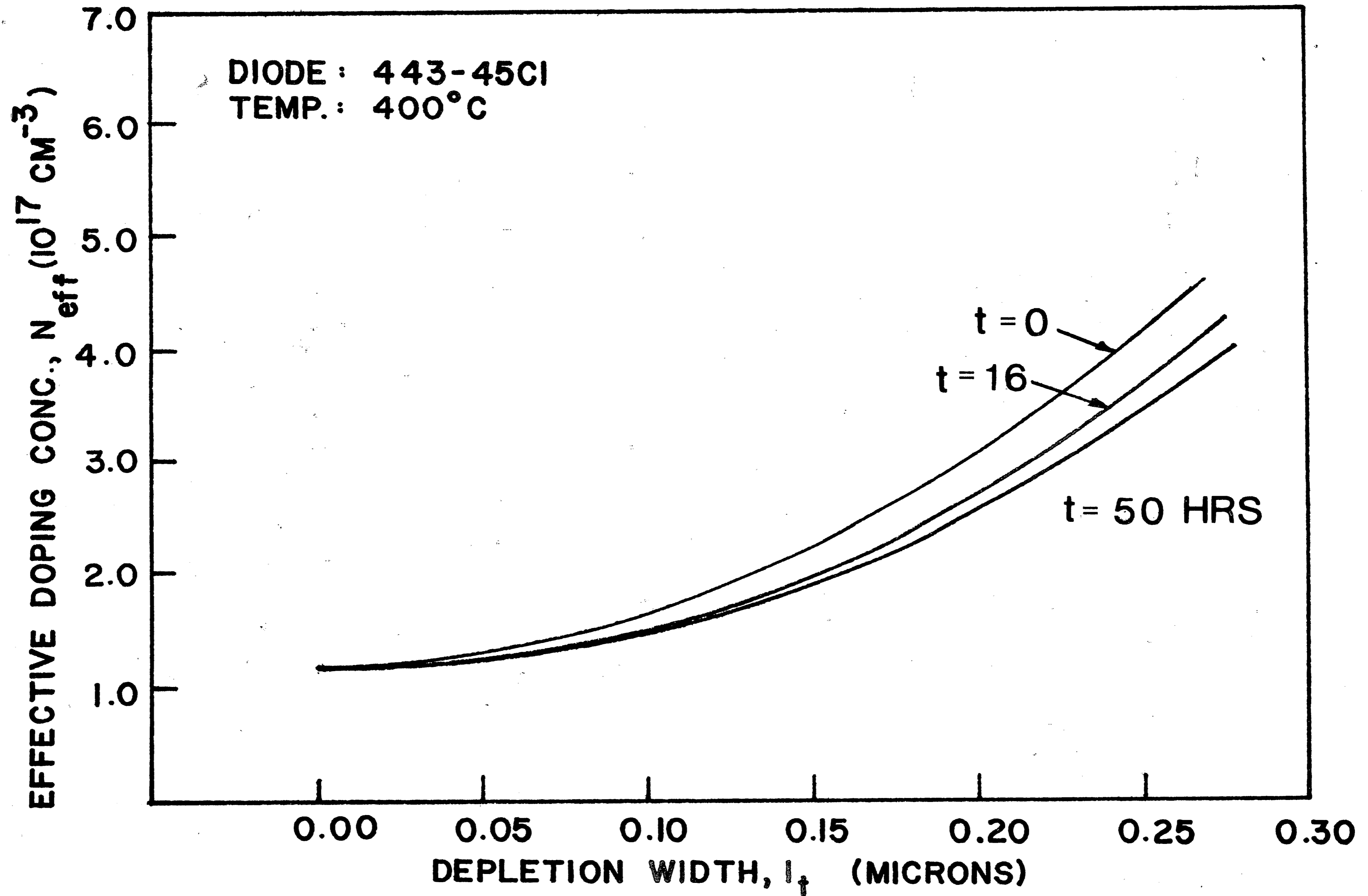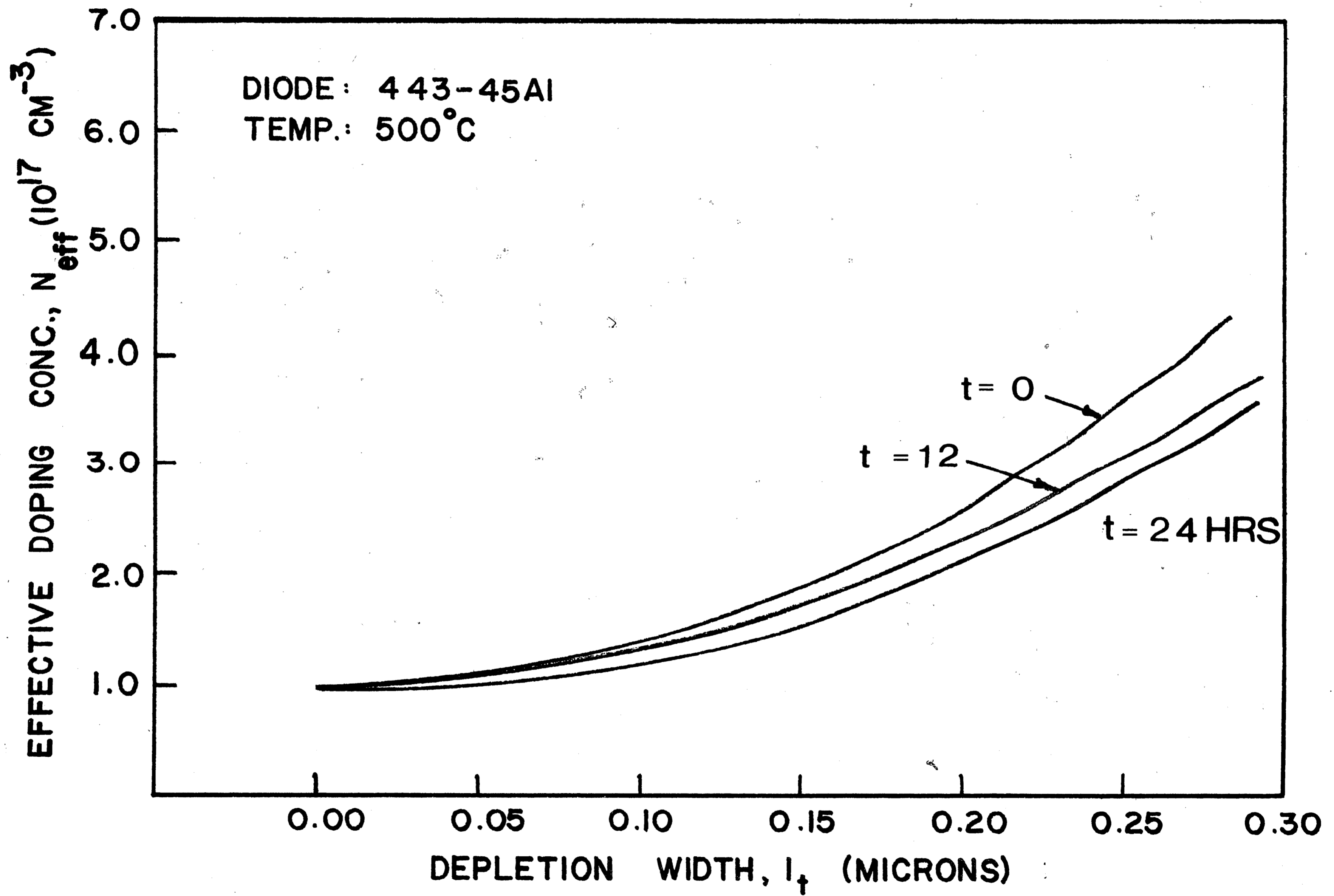
FIGURE 24

FIGURE 25
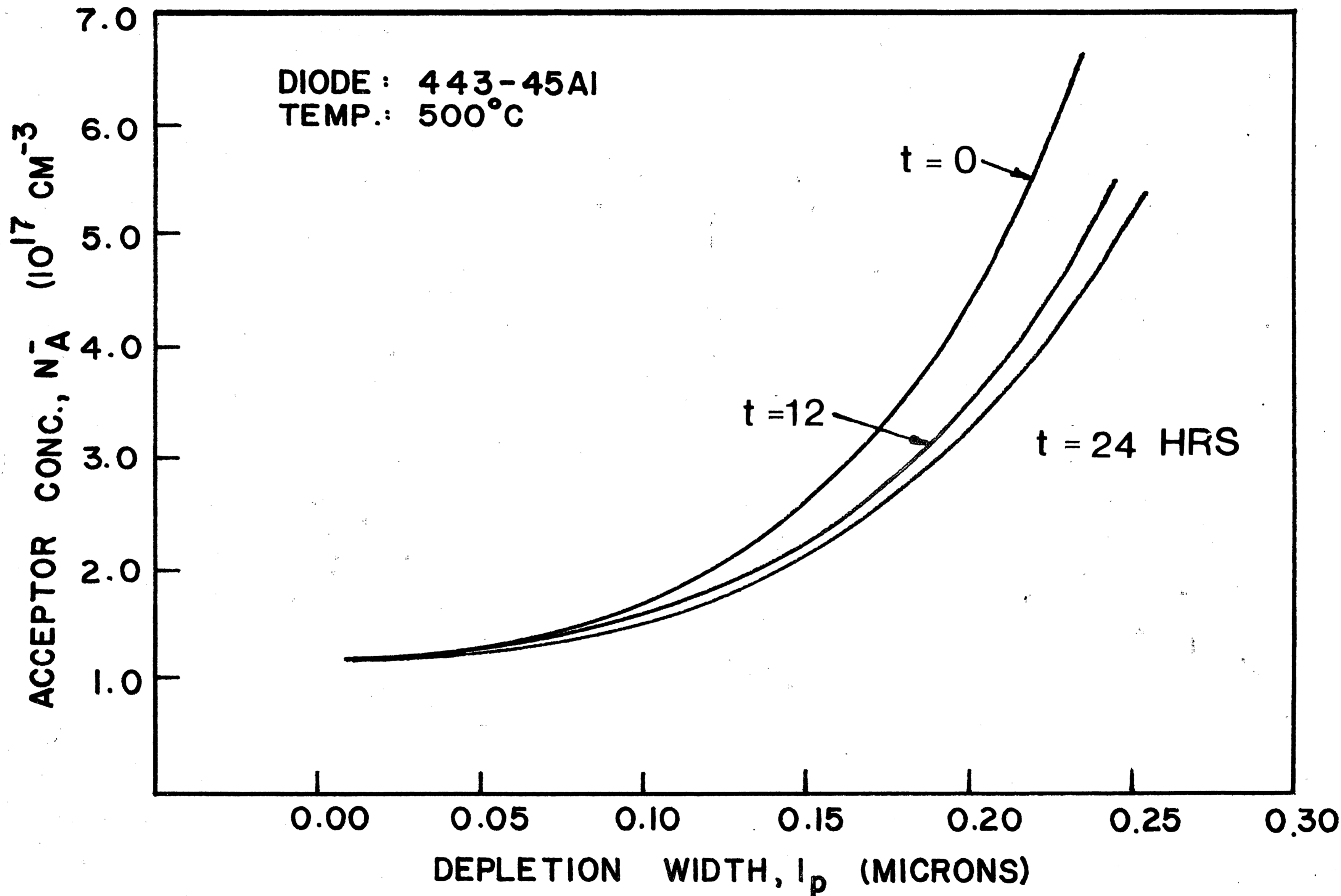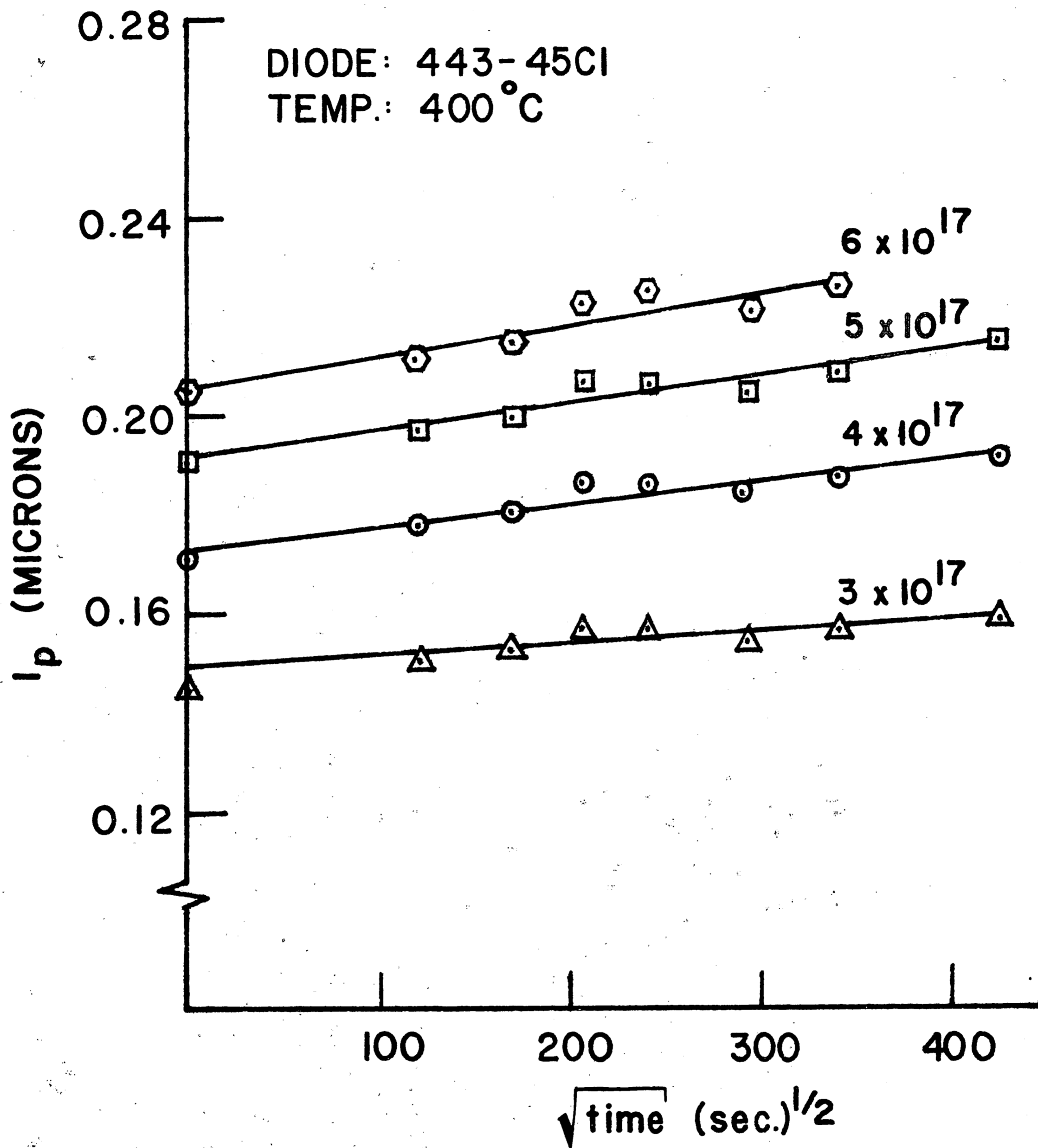
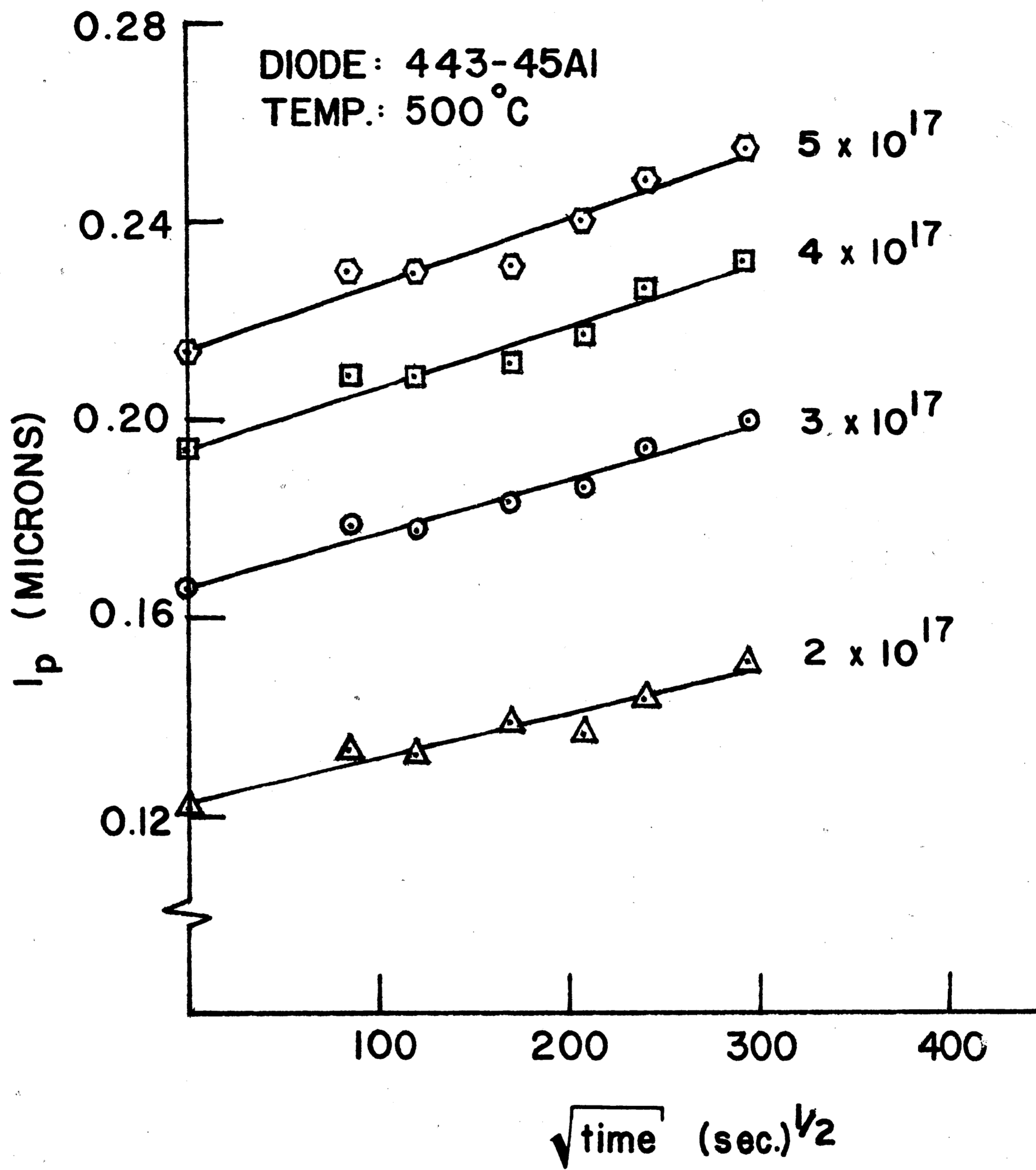FIGURE 26

DIODE: 443-45Al
TEMP.: 500°C

t = 0
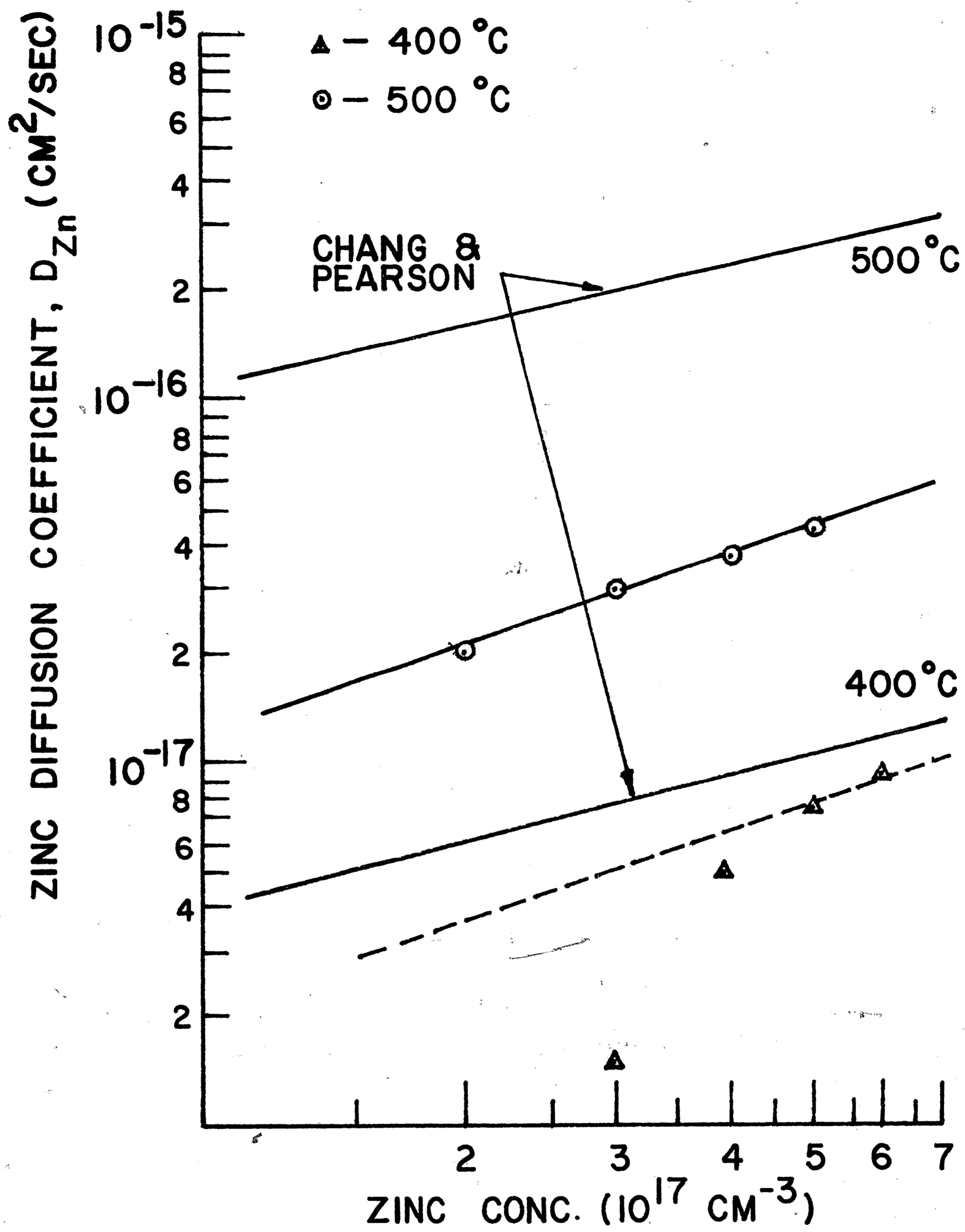
t = 12

t = 24 HRS

FIGURE 27
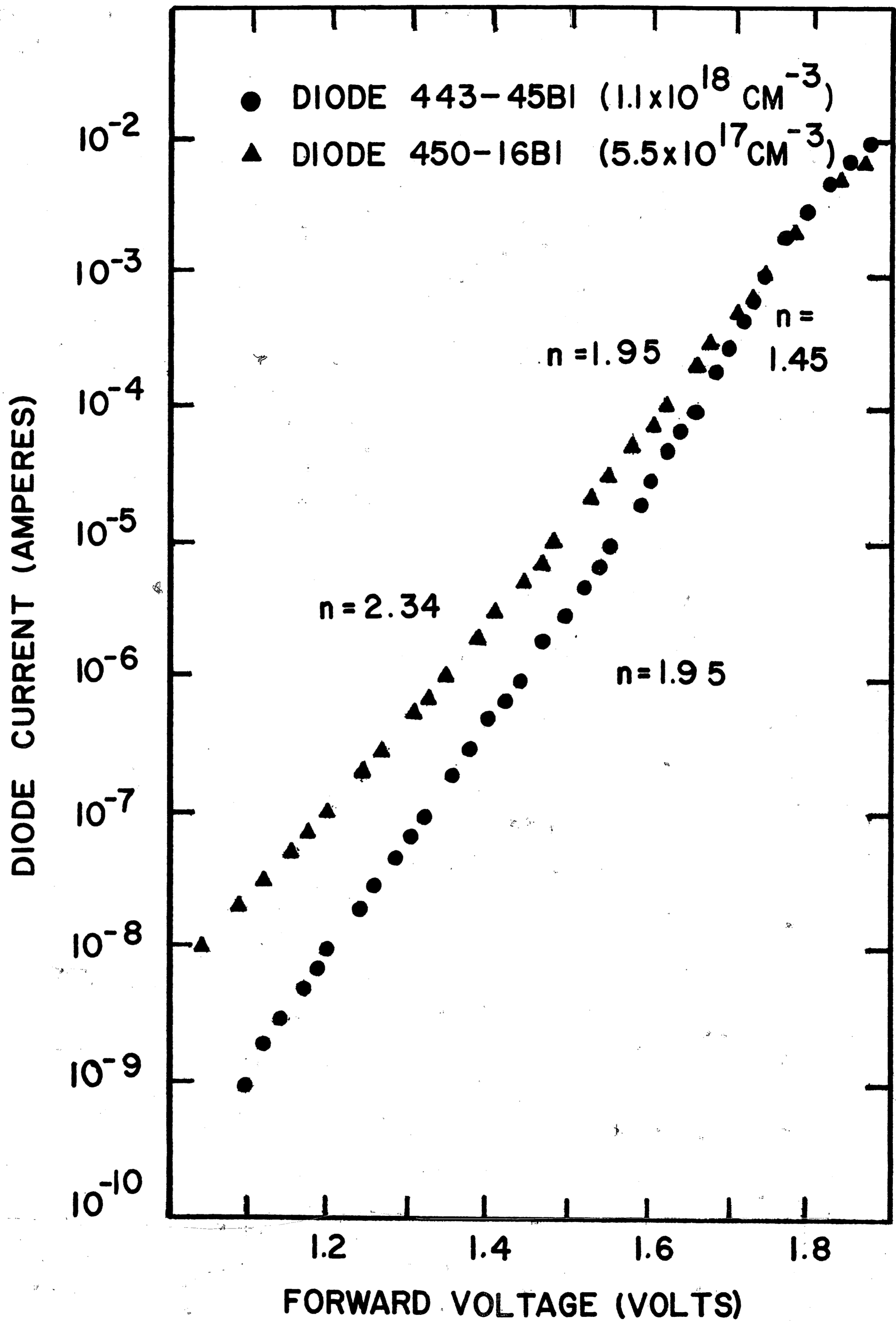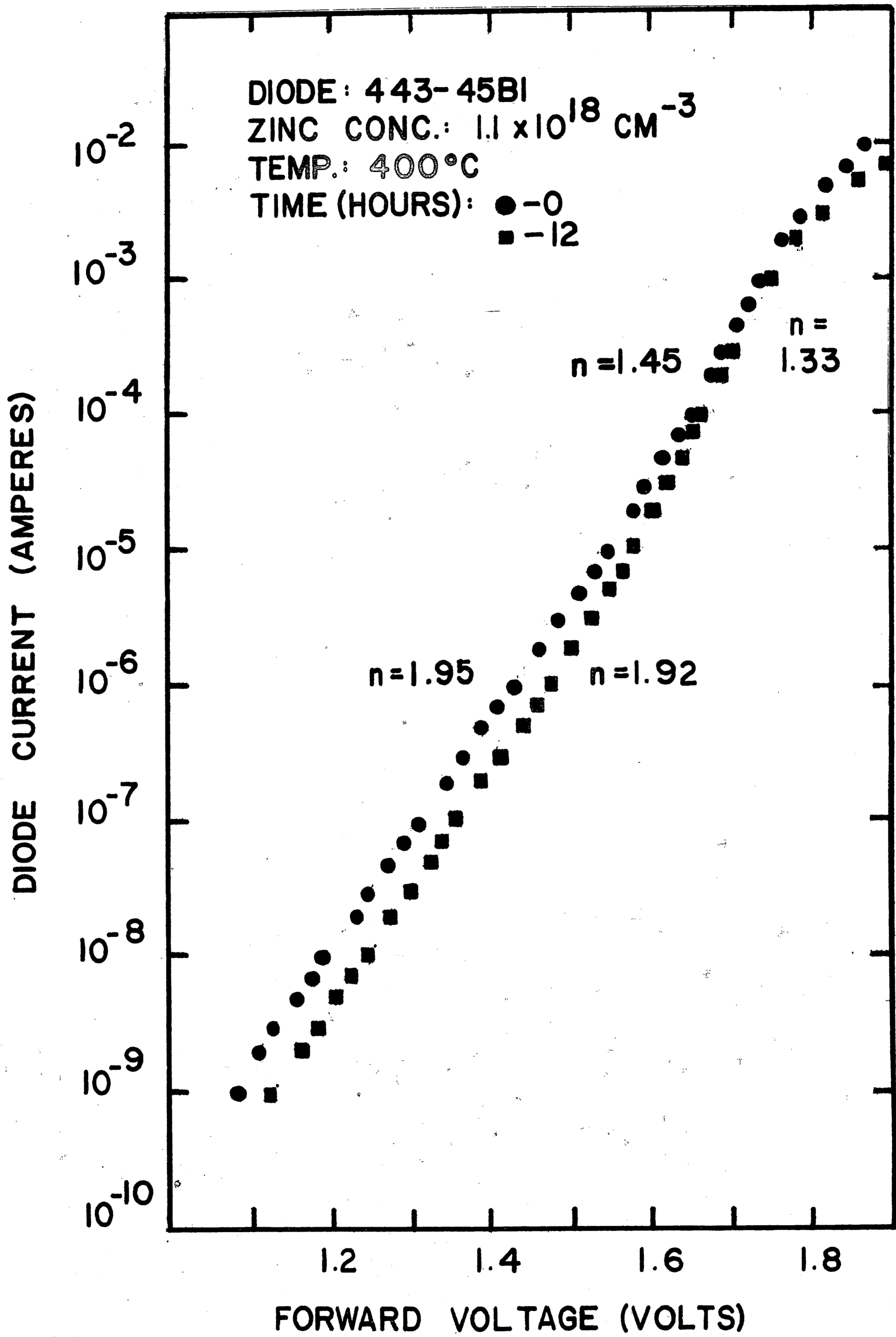
FIGURE 28

FIGURE 29

FIGURE 30
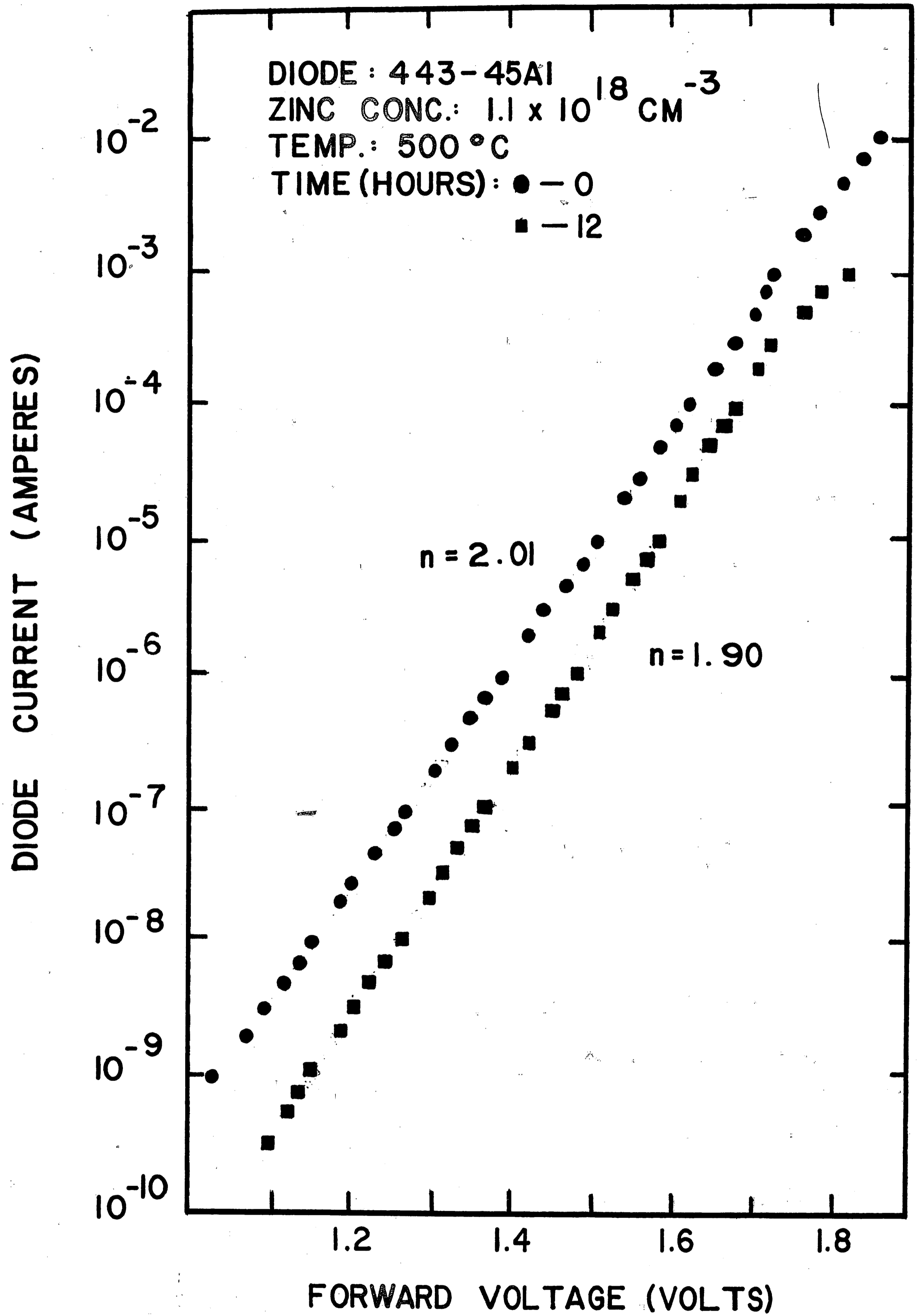
FIGURE 31

FIGURE 32

FIGURE 33

BIBLIOGRAPHY

1. Gershenzon, M. and Mikulyak, R.M., "Electroluminescence at p-n Junctions in Gallium Phosphide", J. Appl. Phys., Vol. 32, p. 1338 (1961).

2. Gershenzon, M. and Mikulyak, R.M., "Light Emission From Forward Biased p-n Junctions in Gallium Phosphide", Solid-State Elect., Vol. 5, p. 313 (1962).

3. Casey, Jr., H.C. and Trumbore, F.A., "Single Crystal Electro-luminescent Materials", Material Sci. Eng., Vol. 6, p. 69 (1970).

4. Henry, C.H., Dean, P.J., and Cuthbert, J.D., "New Red Pair Luminescence from GaP", Phys. Rev., Vol. 166, p. 754 (1968).

5. Morgan, T.N., Webber, B. and Bhargava, R.N., "Optical Properties of Cd-O and Zn-O Complexes in GaP", Phys. Rev., Vol. 166, p. 751 (1968).

6. Cuthbert, J.D., Henry, C.H. and Dean, P.J., "Temperature Dependent Radiative Recombination Mechanisms in GaP(Zn,O) and GaP(Cd,O)", Phys. Rev., Vol. 170, p. 739 (1968).

7. Rosenzweig, W., Hackett, Jr., W.H. and Jayson, J.S., "Kinetics of Red Luminescence in GaP", J. Appl. Phys., Vol. 40, p. 4477 (1969).

8. Bhargava, R.N., "Role of Oxygen in (Zn,O) Doped GaP", Phys. Rev. B, Vol. 2, p. 387 (1970).

9. Dishman, J.M., DiDomenico, Jr., M. and Caruso, R., "Luminescence and Minority Carrier Recombination in P-Type GaP(Zn,O)", Phys. Rev. B, Vol. 2, p. 1988 (1970).

10. Bhargava, R.N., "Time Decay and Temperature Dependence of Radiative Recombination in (Zn,O)-Doped GaP", J. Appl. Phys., Vol. 41, p. 3698 (1970).

11. Dishman, J.M. and DiDomenico, Jr., M., "Recombination Kinetics at Isoelectronic Impurities: GaP(Zn,O)", Phys. Rev. B, Vol. 1, p. 3381 (1970).

BIBLIOGRAPHY (cont.)

12. Chang, L.L., "Diffusion, Solubility and Distribution Coefficient of Zinc and Gallium", Stanford Univ. Ph.D. Thesis(1964).

13. Chang, L.L. and Pearson, G.L., "Diffusion Mechanism of Zn in GaAs and GaP Based on Isoconcentration Diffusion Experiments", J. Appl. Phys., Vol. 35, p. 1960(1964).

14. Chang, L.L. and Pearson, G.L., "Diffusion and Solubility of Zinc in Gallium Phosphide Single Crystals", J. Appl. Phys., Vol. 35, p. 374(1964).

15. Longini, R.L., "Rapid Zinc Diffusion in Gallium Arsenide", Solid-State Elect., Vol. 5, p. 127(1962).

16. Logan, R.A., White, H.G. and Trumbore, F.A., "P-N Junctions in GaP With External Electroluminescence Efficiency 2% at 25°C", Appl. Phys. Letters, Vol. 10, p. 206(1967).

17. Onton, A. and Lorenz, M.R., "Dependence of Radiative Efficiency in GaP Diodes on Heat Treatment", Appl. Phys. Letters, Vol. 12, p. 115(1968).

18. Maeda, K., Kasami, A. Toyama, M. and Wakamatsu, N., "Minority Carrier Lifetime in GaP Electroluminescent Diodes", Jap. J. Appl. Phys., Vol. 8, p. 65(1969).

19. Toyama, M., Kasami, A., Naito, M. and Maeda, K., "Effect of Heat Treatment on Diffused GaP Electroluminescent Diodes", Trans. of the Metallurgical Soc. of AIME, Vol. 245, p. 551 (1969).

20. Toyama, M., Maeda, K. and Sekiwa, T., "Green and Red Electroluminescence from Diffused Gallium Phosphide p-n Junctions", Jap. J. Appl. Phys., Vol. 9, p. 468(1970).

21. White, H.G. and Logan, R.A., "GaP Surface-Barrier Diodes", J. Appl. Phys., Vol. 34, p. 1990(1963).

22. Cowley, A.M., "Depletion Capacitance and Diffusion Potential of Gallium Phosphide Schottky Barrier Diodes", J. Appl. Phys., Vol. 37, p. 3024(1966).

BIBLIOGRAPHY (cont)

23. Peaker, A.R. and Smith, B.L., "The Measurement of Doping
    Profiles in Thick Epitaxial Layers of GaP Using Schottky
    Barrier C-V Data", Solid-State Elect., Vol. 13, p. 1407
    (1970).

24. van Opdorp, C., "Evaluation of Doping Profiles From Capacitance
    Measurements", Solid-State Elect., Vol. 11, p. 397(1968).

25. Saul, R.H., "Effect of Etching on the Efficiency and Emission
    Pattern of Annealed GaP Electroluminescent Diodes", J. Appl.
    Phys., Vol. 40, p. 4978(1969).

26. Schottky, W., "Vereinfacht und Erweiterte Theorie der
    Randschichtgleichrichter", Zeitschrift fur Physik, Vol. 118,
    p. 539(1942).

27. Hackett, Jr., W.H. and Scharfetter, D.L., "Determination of
    Impurity Distribution in n-on-p Liquid-Phase Epitaxially
    Grown LPE Diodes from Analysis of Capacitance-Voltage Data",
    Solid-State Device Research Conf., Univ. of Rochester(1969).

28. Sah, C.T., Noyce, R.N. and Shockley, W., "Carrier Generation
    and Recombination in P-N Junctions and P-N Junction
    Characteristics", Proc. of the IRE, Vol. 45, p. 1228(1957).

29. Morgan, T.N., "Effect of Deep Traps on Capacitance, Current
    and Light Output of Junctions", IEEE Trans. Electron Devices,
    Vol. Ed-11, p. 533(1964).

30. Morgan, T.N., "Luminescence and Recombination Through Defects
    in p-n Junctions", Phys. Rev., Vol. 139, p. A294(1965).

31. Shockley, W., "The Theory of p-n Junctions in Semiconductors
    and p-n Junction Transistors", Bell Sys. Tech. J., Vol. 28,
    p. 435(July 1949).

32. Saul, R.H., Armstrong, J. and Hackett, Jr., W.H., "GaP Red
    Electroluminescent Diodes With an External Quantum Efficiency
    of 7%", Appl. Phys. Letters, Vol. 15, p. 229(1969).

33. Wiley, J.D., "Donor-Acceptor Pairing in the System GaP(An,0)",
    J. Phys. and Chem. Solids, Vol. 32, No. 9, p. 2053(Sept. 1971).

BIBLIOGRAPHY (cont)

34. Hackett, Jr. W.H. and Bhargava, R.N., "Correlation Between Photoluminescence and Electroluminescence Time Decay in Red-Emitting GaP Diodes at Room Temperature", J. Appl. Phys., Vol. 41, No. 8, p. 3306(July 1970).

35. Logan, R.A. and Chynoweth, A.G., "Charge Multiplication in GaP p-n Junctions", J. Appl. Phys., Vol. 32, p. 1649(1962).

36. Grove, A.S., Physics and Technology of Semiconductor Devices, John Wiley and Sons, Inc., New York, N.Y., 1967.

37. von Rosenberg, D.U., Methods for the Numerical Solution of Partial Differential Equations, American Elsevier Pub. Co., Inc., New York, N.Y., 1969.

38. Hackett, Jr., W.H., McGahan, T.E., Dixon, R.W. and Kammlott, G.W., "A Scanning Electron Microscope Investigation of Etching Phenomena in GaP Electroluminescent Diodes", J. Electrochem. Soc., July 1972(to be published).

39. Kleinman, D.A., "The Forward Characteristic of the PIN Diode", Bell Sys. Tech. J., Vol. 35, p. 685(1956).

40. Sze, S.M., Physics of Semiconductor Devices, John Wiley and Sons, Inc., New York, N.Y., 1969.

VITA

Robert A. Worden was born on December 20, 1942 in Independence, Missouri to Mr. and Mrs. Emery A. Worden.

Mr. Worden was graduated from Van Horn High School in Independence, Missouri in June 1960. After graduation he enrolled at Metropolitan Junior College in Kansas City, Missouri. He attended Metropolitan Junior College, while working full-time at Armco Steel Corporation in Kansas City, until June 1965. In September 1965 he enrolled in the Department of Electrical Engineering at the University of Kansas located in Lawrence, Kansas.

Upon graduation in June 1968 with the degree of Bachelor of Science in Electrical Engineering, Mr. Worden was employed by Western Electric in Lee's Summitt, Missouri as a Planning Engineer in the Wafer Preparation area. In his assignment Mr. Worden was responsible for the diffusion, passivation and contacting of silicon switching transistors.

Since July 1970 he has been a Lehigh Master's candidate assigned to Western Electric's Engineering Research Center located in Princeton, New Jersey. His assignment is involved with the characterization of the electrical and optical properties of GaP light-emitting diodes.

Mr. Worden is married to the former Katherine Ann Gallup of Independence, Missouri and has an eight year old son, Phillip.